MARMARA UNIVERSITY

FACULTY OF ENGINEERING

MODELING OF CORRUGATED TUBE EVAPORATORS IN CO2 (R744) FLUID TRANSCRITICAL REFRIGERATION CYCLES

Ecem ÇOLAK, Neslihan KILIÇARSLAN

Müdek Final Project Commission

The essential features of an acceptable design Project

		Satisfied	Unsatisfied
1	Mechanical or Thermal Design	✓	
2	Report writing technique	✓	
3	Development of student creativity		☑
4	Use of open-ended problems		☑
5	Formation of design	✓	
6	Problem statement and specification	✓	
7	Synthesis of alternative solutions		☑
8	Feasibility	✓	
9	Detailed system description	✓	
10	Consideration of constraints (e.g. economic, safety, reliability, etc.)		☑
11	Utilization of engineering and scientific principle	✓	

Decision	Signature
Accepted but not approved	19.07.2021
Prof. Dr. Bülent Ekici,	
Dr. Öğr. Üyesi Uğur Tümerdem	
Ar. Gör Serkan Öğüt	

GRADUATION PROJECT REPORT

Department of Mechanical Engineering

Supervisor

Dr. Mehmed Rafet ÖZDEMİR

ISTANBUL, 2021

MARMARA UNIVERSITY

FACULTY OF ENGINEERING

Modeling of Corrugated Tube Evaporators in CO2 (R744) Fluid Transcritical Refrigeration Cycles

by

Ecem ÇOLAK, Neslihan KILIÇARSLAN

July, 2021, Istanbul

SUBMITTED TO THE DEPARTMENT OF MECHANICAL ENGINEERING IN PARTIAL FULFILLMENT OF THE REQUIREMENTS FOR THE DEGREE

OF

BACHELOR OF SCIENCE

AT

MARMARA UNIVERSITY

Signature of Author(s)

Department of Mechanical Engineering

Certified By Asst. Prof. Dr. Mehmed Rafet ÖZDEMİR .....

Project Supervisor, Department of Mechanical Engineering

Accepted By Prof Dr Bülent EKİCİ .....

Head of the Department of Mechanical Engineering

ACKNOWLEDGEMENT

To begin with of all, we would like to thank our administrator Mehmed Rafet ÖZDEMİR, for the profitable direction and advice on planning this proposition and giving our moral and material support. We would like to thank TÜBİTAK for supporting us inside the degree of the Undergraduate Research Projects Support Program for Industry. We would too like to thank Friterm A.Ş for their support of our industry-partnered project.

July, 2021 Ecem Çolak, Neslihan Kılıçarslan

CONTENT

ABSTRACT

Modeling of Grooved Tube Evaporators in CO2 (R744) Fluid Transcritical Refrigeration Cycles

CO2 was utilized extensively within the refrigeration industry for a period of time. In any case, due to the thermophysical properties of high critical pressure and low critical temperature and the decrease in heat transfer coefficient caused by these, halocarbon refrigerants have been supplanted. In any case, afterward, due to the negative impacts of halocarbon refrigerants on the environment, it has been reused as an elective, natural refrigerant. With the creating innovation, different studies have been performed to extend the effectiveness of CO2 transcritical refrigeration cycles.

One of them is the threading of the evaporator pipes. The most important advantage of using grooved pipe is increasing of the heat transfer coefficient compared to straight pipe units. Thus, the increase in the heat transfer coefficient increases the capacity of the product when the internally threaded pipe unit of the same pipe length is compared with the straight pipe unit. However, the biggest disadvantage of using grooved pipes is the increase in pressure loss. Modeling of different groove geometries to make the system more efficient will shed light on future studies and will enable the development of systems with minimum pressure and maximum heat transfer coefficient.

In this project, internally threaded pipes used in the evaporator in the CO2 transcritical refrigeration cycle will be modeled in computational fluid dynamics programs using different thread geometries. After the model has been experimentally verified, model results will be obtained for at least four different designs with different thread count, apex angle, helix angle, and pipe diameter.

Keywords: CO2, R744, transcritical cycle, evaporator, natural fluid, threaded pipe

SYMBOLS

Bd : Bond number, = $\frac{g(\rho_l - \rho_g){D_i}^2}{\sigma}$

Bo : Boiling number, = $\frac{q^{"}}{G\, i_{fg}}$

Di : inner diameter, m

E : enhancement factor

G : gravitational acceleration, $m\ s^{-2}$

h : heat transfer coefficient, $W\ m^{-2}\ K^{-1}$

i : enthalpy, $J\ kg^{-1}$

k : thermal conductivity, $W\ m^{-1}\ K^{-1}$

M : molecular weight, $kg\ kmol^{-1}$

P : pressure, Pa

P* : reduced pressure

Pr : Prandtl number, = $\frac{\mu\, c_p}{k}$

Re : Reynolds number, = $\frac{G\ D}{\mu}$

S : suppression factor

T : temperature, K

u_m : mean velocity, $m\ s^{-1}$

x : quality

X : Martinelli parameter, = $\left(\frac{1-x}{x}\right)^{0.9}\left(\frac{\rho_g}{\rho_l}\right)^{0.5}\left(\frac{\mu_l}{\mu_g}\right)^{0.1}$

WeD: Weber number, = $\frac{\rho_g {u_m}^2 D_i}{\sigma}$

Θ_{dry} : dry angle

Φ^2 : two phase multiplier

τ^2 : dimensionless physical property coefficient

ρ : density, $kg\ m^{-3}$

σ : surface tension, $N\ m^{-1}$

ABBREVIATIONS

CFC : Chlorofluorocarbon

CFD : Computational Fluid Dynamics

GWP : Global Warming Effect

HC : Hydrocarbon

HCFC : Hydrochlorofluorocarbon

HFC : Hybrid Fiber Coaxial

HTC : Heat Transfer Coefficient

ODP : Ozone Depletion Potential

REFPROP : Reference Fluid Properties

RNG : Re-Normalization Group

SST : Shear Stress Transport

W.R.T. : With Respect To

LIST OF FIGURES

LIST OF TABLES

1. INTRODUCTION

The use of CO2(R744) refrigerant in cooling cycles in air conditioning systems is very important for global warming and sustainable environment.

The research question of the project; Can the modeling of the corrugated pipes used in the evaporator, which is an important element in transcritical refrigeration systems with R744 operating under high pressure, be done correctly in accordance with the experiments?

Corrugated pipe is a product that is used in products in the air conditioning sector and has positive and negative effects. Its most important advantage is that the heat transfer coefficient of the fluid side is higher than straight pipes. This increase also has a positive effect on the product capacity.Higher pressure loss than straight pipes is the negative aspect of corrugated pipes.[7]

The advantages and disadvantages of straight pipe and grooved pipe preferences have been studied in many studies.There are also studies on corrugated pipe geometries that can be made more efficient with suitable geometries, as well as changing the preference rates according to product types.

In this project, in which CO2 is used unlike other fluids, corrugated pipe geometries with this fluid, which has different thermophysical properties, it was aimed to model efficient geometries and to obtain close results by comparing them with the results in the literature.

The goal of the project; It is possible to verify the results with correlation results by modeling the corrugated pipes with different apex angle and helix angle used in evaporator coils with the computational fluid dynamics method. On the other hand, the effects of apex angle and helix angle on heat transfer and pressure drop can be analyzed parametrically.

The main objectives of the project are;

1-To calculate the heat transfer coefficient and pressure loss by changing the Reynold numbers using the correlation equations accepted in the literature.

2-To perform flow analysis of a selected corrugated pipe models and straight pipe model via ANSYS Fluent program and to perform model analysis.

3-To reveal the effects of apex angle and helix angle parameters on the heat transfer coefficient and pressure drop.

1.1. General Information

As the negative effects of halocarbons on the environment have been noticed, the use of natural refrigerants has started to come to the fore. The Global Warming Effect -Ozone Depletion Potential values for different gases are given in Table 1. CO2 with a GWP of 1 and an ODP of 0 is a pretty good option.

Table 1.1. GWP and ODP Values for Different Refrigerants

Refrigerants	GWP(According to CO_2 ,100 years)	ODP (According to R11)	Atmospheric holding time (year)
R11	3.800	1	50
R12	8.100	1	102
R13b1	5.400	10	65
R22	1.500	0.055	13.3
R23	12.000	0	260
R134a	1.300	0	13.6
R717-Ammonia	0	0	-
R744-CO_2	1	0	-
R290-Propane	3	0	-

In today's conditions, where environmental effects are very important, CO_2 can be turned into an efficient gas despite its thermophysical properties, thanks to technological improvements.

It is known that the properties of CO2 are distinctive from other ordinary refrigerants. By comparison, the foremost striking highlight of CO2 is its low critical point temperature (31.06 °C) and high pressure (73.8 bar) [2]. Another constraining factor in applying CO2 is its high triple point at -56.6 °C and a corresponding 5.1 bar pressure. Additionally, when compared to ordinary liquids (CFC, HCFC, HFC, HC), the vapor pressure and volumetric heat transfer capacity (22545 kJ/m3 at 0°C) are very high.[3]

As can be seen from the CO2 phase graph, there are three states where two phases are in balance: Solid-Gas, Solid-Liquid, Liquid-Gas balance states. Under climatic pressure, CO2 can as it were existing in solid or vaporous frame. At this pressure, the fluid phase is not conceivable. Over this temperature, CO2 sublimes into the gas phase. It is the condition

where the three states of 5.2 bar and -56.6°C CO2 are in harmony. Under these conditions, the three states of matter are in balance. At 31.1°C, CO2 comes to the critical point. At this point, the densities of the fluid and gas stages are break even with and the contrast between the two stages disappears. As a result, a new stage rises. This stage of matter is called the supercritical phase. CO2 Phase Graph is given in Figure 1, CO2 lnP – h Graph is given in Figure 2 [2,4].

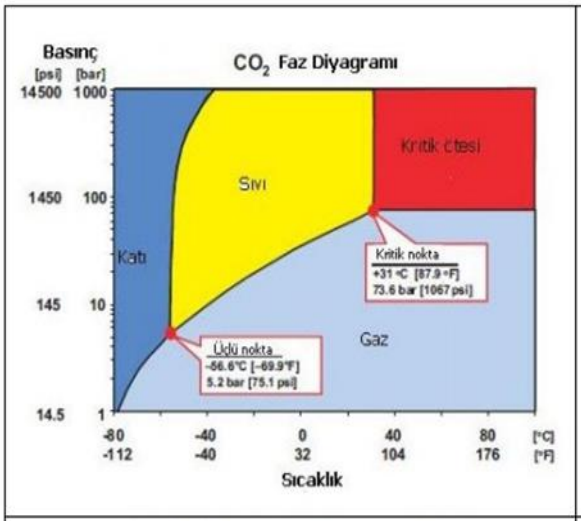

Figure 1.1. CO_2 Phase Diagram [2]

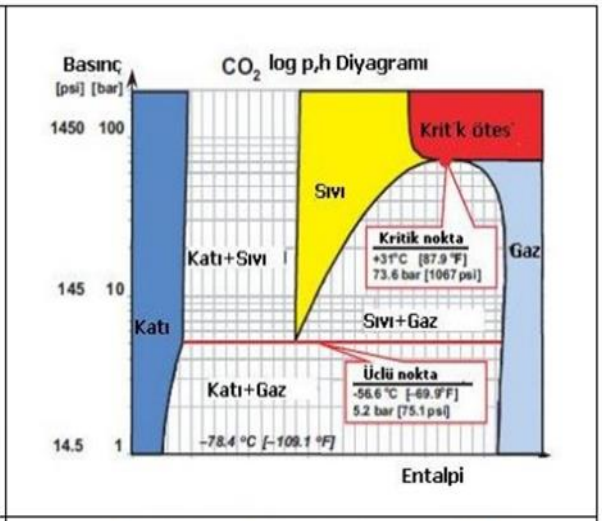

Figure 1.2. CO_2 Log p,h Diagram [2]

As could be seen from Table 1.2., CO2 has appealing thermophysical properties and low viscosity, high volumetric capacity, high thermal conductivity, and high vapor density compared to halocarbon refrigerants [2,5,6].

Table 1.2. Thermophysical Properties of Commonly Known Refrigerants

Refrigerants	Tcritical, (°C)	Pcritical, (bar)	Liquid Phase Density ρf,(kg/m3) [a]	Vapour Phase Density (kg/m3) [b]	Thermal Capacity cp, (kJ/kg) [a]	Volumetric Capacity (kJ/m3) [a]	Heat Conduction Coefficient k, (W/m.K) [a]	Dynamic Viscosity μ,(mPa.s) [a]
R11	198	44.1	1536.9	2.36	0.85	450.76	0.09	0.5
R12	112	42.2	1400.1	17.185	0.93	2636.52	0.62	0.25
R22	96.2	49.9	1285.7	20.41	1.16	4205.28	0.09	0.22
R134a	101.1	40.6	1298.9	13.9	1.3	2773.75	0.09	0.27

R410a	72.13	49.3	1175	28.82	1.5	6566.35	0.1	0.16
R404a	72	37.3	1154.8	29.91	1.3	4953.99	0.07	0.18
R407c	86.74	46.2	1240.8	18.86	1.4	3973.24	0.01	0.21
R507a	70.6	37.05	1161.1	30.98	1.37	5055.32	0.072	0.18
R744 (CO2)	**31**	**73.7**	**934.26**	**94.148**	**2.5**	**22089.00**	**0.11**	**0.101**
R717 (NH3)	132.3	113.3	640.28	3.31	4.41	4192.51	0.56	0.172

Remarks: [a] saturated liquid at -1.1°C; [b] Saturated steam at -1.1°C

Pipe geometry is also a very important point to improve the effectiveness of the evaporator. Straight pipe and corrugated pipe are used in such devices. The reason why the corrugated pipe is generally preferred is that it has more wetted portion surface than the straight pipe and creates turbulence, thus increasing the heat transfer coefficient.

However, the corrugated pipe also has some disadvantages due to pressure loss and friction. Parameters such as helix angle, apex angle, thread height, thread number, pipe diameter in the grooved pipe geometry are of great importance in the design [7]. These parameters should be modeled in order to form a basis for future studies. CO2 has a two-phase flow in this cycle. Two-phase flow is quite complex compared to single-phase flow.

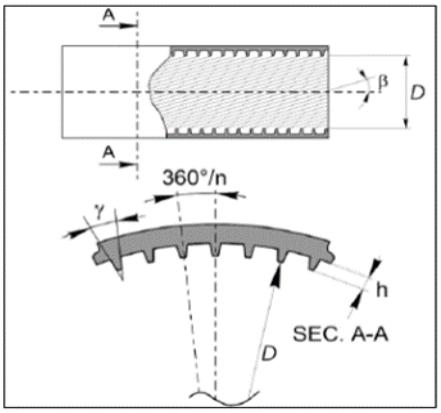

Figure 1.3. Corrugated Pipe Geometry [7]

Evaporation is a physical mechanism with two-phase flow conditions. The fact that the physical properties between the phases are very different (for example, the density difference size) in two-phase flow makes it difficult to calculate the heat transfer and pressure drop correctly. For the same condition, studies examining the two-phase flow relations in the literature emphasized that the results gave very different results from each other. This is due to the limited experimental conditions made while obtaining the relations. Therefore, studies on obtaining and modeling general two-phase flow relations are still up-to-date. In the

literature, the number of studies on corrugated pipes for the evaporation of CO2 is not very large.

As it can be seen from the literature research above, although the number of studies examining the evaporation of pure CO2 in grooved pipes is few, there is not a very good agreement between the correlations. Calculations can be made with appropriate correlations. The results of the analysis will be compared with the theoretical calculations. The validated model will reveal the effects of apex angle and helix angle on the heat transfer coefficient and pressure drop for single phase flow.

2. LITERATURE SEARCH

2.1 Heat Transfer Coefficient Research for One Phase Flow

By reason of the abrupt alteration within the thermophysical properties of the CO2 with temperature and pressure, the heat transfer coefficient of the fluid through the abrupt peak region might obtain different results [24]. These points where the specific heat and heat transfer coefficient suddenly reach their peaks are called pseudocritical**.** [33,21].The researchers stated that specifying the correlation of the supercritical CO2 heat transfer coefficient in the pseudo-critical region is impossible [23,21].

Nusselt correlation which developed based on numerical and experimental research can be used to examine the heat transfer of CO2 fluid within this area.

These correlations are tested at different Reynolds number ranges and for different design conditions [21] .

In this section, correlations found in the literature and used in thesis calculations are listed.

2.1.1 Dittus-Boelter Correlation

Dittus and Boelter conducted a correlation study to examine the Nusselt numbers in turbulent flow for supercritical CO2 in horizontal smooth pipe.

With these studies, correlation revealed via variation of Reynold and Prandtl numbers depending on free flow temperature [21,22].

$$\mathrm{Nu} = 0.023 * \mathrm{Re}^{0.8} * \mathrm{Pr}^{0.4} \quad (1)$$

2.1.2 Gnielinski Correlation

Gnielinski repeated the correlation study to adjust the Nusselt number within turbulence and created a new empirical correlation [20,21].

$0.5 \leq \mathrm{Pr} \leq 2000$

$3000 \leq \mathrm{Re_{Dh}} \leq 5 \times 10^6$

$$\mathrm{Nu_G} = \frac{\left(\frac{\mathrm{f}}{8}\right) * (\mathrm{Re} - 1000)\mathrm{Pr}}{1.07 + 12.7(\mathrm{f}/8)^{\frac{1}{2}}(\mathrm{Pr}^{\frac{2}{3}} - 1)} * \left[1 + \left(\frac{\mathrm{D_H}}{\mathrm{L}}\right)^{\frac{2}{3}}\right] \quad (2)$$

Where ;

$\mathrm{D_H} =$ The hydrolic diameter (m)

$\mathrm{Re} =$ the Reynolds Number

$\mathrm{Pr} =$ the Prandtl Number

$\mathrm{Nu} =$ the Nusselt Number

$\mathrm{f} =$ the Darcy friction factor

In this part, the pressure drop formula used in the project and the correlations used for single-phase flow are listed.

2.2 Pressure Drop for Single Phase Flow Research

Pressure drop in straight pipes could be calculated with the formula below. [19]

$$\Delta P = f * \frac{L}{D} * \frac{\rho * V_m^2}{2} \quad (3)$$

Where:

ρ = fluid density in kg per cubic meter

L = Length of pipe (m)

D = Pipe diameter(m)

V_m = Mean flow velocity $(\frac{m}{s})$

f=Darcy friction factor calculated below Blasius Equation

$$f = \frac{0.316}{Re^{0.25}} \tag{4}$$

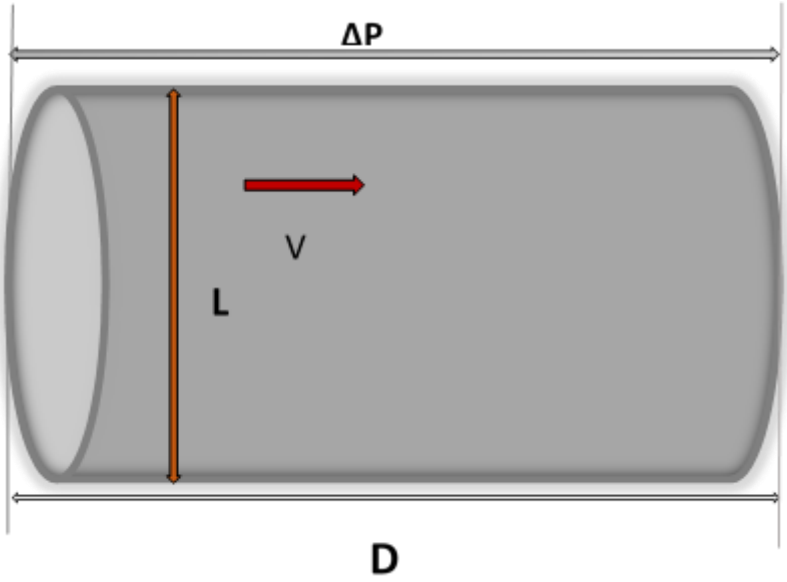

Figure 2.1. Pressure drop formula visual representation

2.3 Heat Transfer Coefficient Research for Two Phase Flow in Smooth Pipe

This section lists the important two phase straight pipe correlations.

Information about the Fang correlation, which has the widest range of use among all correlations, is detailed below.

Looking at Fang's database-based study of 2956 data points for CO2 experimental boiling heat transfer coefficient in 2013 and his second study in 2017, which consisted of 17.778 data, it can be said that there are studies with a wide flow regime and geometry range.

The fact that more than 80% of the collected 5223 data obtained results with an error range of 30% also proves that the correlation has a good approach.

The correlations of wide diameter, temperature, heat flux and mass flux range, and low error rate are quite good for two-phase flows in straight pipes. When used in mini or macro channels, its accuracy will not change significantly. [11]

Table 2.1. Flow boiling heat transfer empricial correlations from different studies for pure carbon dioxide in smooth tubes [11]

Author	Formulation	Range of applicability
Hwang et al. (1997)	$h = Sh_{nb} + Eh_{cb}$ Nucleate boiling heat transfer coefficient h_{nb} with Forster and Zuber (1955) correlation $h_{cb} = Pr_L^{0.6} \cdot h_L$, liquid heat transfer coefficient h_L with Dittus and Boelter (1930) correlation $E = 2 \cdot (0.213 + {}^{1}/_{X_{tt}})^{0.736}$ for $X_{tt} < 10$ $E = 1$ for $X_{tt} \geq 10$ $S = \frac{1-\exp(-E \cdot h_L \cdot {}^{X}/_{\lambda_L})}{E \cdot h_L \cdot {}^{X}/_{\lambda_L}}$ $X = 0.05 \cdot \sqrt{\frac{\sigma}{g(\rho_L - \rho_V)}}$	$d = 7.0\ mm$ $200 \leq G \leq 400\ kg\ m^{-2}s^{-1}$ $3.0 \leq q \leq 9.0\ kW\ m^{-2}$ $-25 \leq T_{sat} \leq 5\ ^{\circ}C$
Hihara and Tanaka (2000)	$h = (14700 \cdot Bo + 0.93 \cdot ({}^{1}/_{X_{tt}})^{2/3}) \cdot h_{LO}$, with h_{LO} evaluated with liquid-only Dittus and Boelter (1930) correlation.	$0.7 \leq d \leq 2\ mm$ $360 \leq G \leq 1440\ kg\ m^{-2}s^{-1}$, q and T_{sat} ranges not available
Yoon et al. (2004)	$x_{cr} = 38.27 \cdot (Re_L)^{2.12} \cdot (1000Bo)^{1.64} \cdot Bd^{-4.7}$ For $x \leq x_{cr}$ $h = [(Sh_{nb})^2 + (Eh_L)^2]^{1/2}$, with nucleate boiling h_{nb} and liquid h_L heat transfer coefficients evaluated with Cooper (1984) and Dittus and Boelter (1930), respectively. $E = [1 + 9.36 \cdot 10^{3} \cdot \mathrm{Pr}_L(\frac{\rho_L}{\rho_V} - 1)]^{0.11}$ $S = (1 + 1.62 \cdot 10^{-6} \cdot E^{0.69} \cdot \mathrm{Re}_L^{1.11})^{-1}$ For $x > x_{cr}$ $h = \frac{\theta_{dry} h_V + (2\pi - \theta_{dry}) E h_L}{2\pi}$, liquid and vapor heat transfer coefficients with Dittus and Boelter (1930) equation. $E = 1 + 3000Bo^{0.86} + 1.12(\frac{x}{1-x})^{0.75}(\frac{\rho_L}{\rho_V})^{0.41}$ $\frac{\theta_{dry}}{2\pi} = 36.23\mathrm{Re}_L^{3.47} Bo^{4.84} Bd^{-0.27} ({}^{1}/_{X_{tt}})^{2.6}$	$d = 7.73\ mm$ $212 \leq G \leq 530\ kg\ m^{-2}s^{-1}$ $12.3 \leq q \leq 18.9\ kW\ m^{-2}$ $-4 \leq T_{sat} \leq 20\ ^{\circ}C$
Thome and El Hajal (2004)	$h = \frac{\theta_{dry} h_V + (2\pi - \theta_{dry}) h_{wet}}{2\pi}$, the dry angle θ_{dry} varies from 0 in case of annular flow u to θ_{strat} in case of fully stratified flow. The two angles expressions are available in Kattan et al. (1998a, 1998b) $h_V = 0.023(\frac{GxD}{\alpha \mu_V})^{0.8} \mathrm{Pr}_V^{0.4} \frac{\lambda_V}{d}$, in which the void fraction is obtained with Rohuani and Axelsson (1970) model. $h_{wet} = [(Sh_{nb,CO_2})^3 + h_{cb}^3]^{1/3}$ $h_{nb,CO_2} = 0.71 h_{nb} + 3970$, with nucleate boiling heat transfer coefficient calculated with Cooper (1984) equation. $S = \frac{(1-\chi)^{0.5}}{0.121 \mathrm{Re}_{LF}^{0.225}}$ $\mathrm{Re}_{LF} = \frac{4G(1-\chi)\delta}{(1-\alpha)\mu_L}$ $\delta = \frac{d}{4}(1-\alpha)$ $h_{cb} = 0.0133 \cdot \mathrm{Re}_{LF}^{0.69} \mathrm{Pr}_L^{0.4} \frac{\lambda_L}{\delta}$	$0.79 \leq d \leq 10.06\ mm$ $85 \leq G \leq 1440\ kg\ m^{-2}s^{-1}$ $5 \leq q \leq 36\ kW\ m^{-2}$ $-25 \leq T_{sat} \leq 25\ ^{\circ}C$
Pettersen (2004)	For $x \leq x_{cr}$: $h = (h_{nb}^3 + h_{cb}^3)^{1/3}$, with nucleate boiling heat transfer coefficient h_{nb} evaluated with Cooper (1984) equation and the convective boiling heat transfer coefficient estimated with Kattan et al. (1998a, 1998b) flow pattern based model. Post-dryout region ($x \geq x_{cr}$) heat transfer coefficient calculated with Shah and Siddiqui (2000) model. Dryout vapor quality x_{cr} using Kon'kov (1965) expression for H_20 and Ahmad (1973) fluid-to-fluid scaling model	$d = 0.8\ mm$ $190 \leq G \leq 570\ kg\ m^{-2}s^{-1}$ $5 \leq q \leq 20\ kW\ m^{-2}$ $0 \leq T_{sat} \leq 25\ ^{\circ}C$
Choi et al. (2007)	$h = Sh_{nb} + Eh_L$, with nucleate boiling h_{nb} and liquid h_L heat transfer coefficients evaluated with Cooper (1984) and Dittus and Boelter (1930), respectively. $S = 7.2694(\phi^2)^{0.0094} Bo^{0.2814}$ $E = 0.05 \cdot (\phi^2) + 0.95$ $\phi^2 = 1 + \frac{C}{X_{tt,Choi}} + \frac{1}{X_{tt,Choi}^2}$, with the Chisholm parameter C set to 20, 12, 10 and 5 in case of liquid-vapor flow condition of turbulent-turbulent, laminar-turbulent, turbulent-laminar and laminar-laminar, respectively $X_{tt,Choi} = (\frac{1-x}{x})^{7/8} (\frac{\rho_V}{\rho_L})^{0.5} (\frac{\mu_L}{\mu_V})^{1/8}$.	$1.5 \leq d \leq 3.0\ mm$ $400 \leq G \leq 500\ kg\ m^{-2}s^{-1}$ $30 \leq q \leq 40\ kW\ m^{-2}$ $-10 \leq T_{sat} \leq -5\ ^{\circ}C$
Choi et al. (2007)	Same expression as Choi et al. (2007), with a different evaluation of the suppression and enhancement factors: $S = 469.1689(\phi^2)^{-0.2093} Bo^{0.7402}$ $E = 0.042 \cdot (\phi^2) + 0.958$	$1.5 \leq d \leq 3.0\ mm$ $200 \leq G \leq 600\ kg\ m^{-2}s^{-1}$ $10 \leq q \leq 40\ kW\ m^{-2}$ $T_{sat} = 10\ ^{\circ}C$ $fluids: CO_2, R134a, R22$

Cheng et al. (2008a, 2008b)	For any flow pattern except dryout and mist flow: $h = \frac{\theta_{dry} h_V + (2\pi - \theta_{dry}) h_{wet}}{2\pi}$, vapor heat transfer coefficient h_V with Dittus and Boelter (1930) equation. $\theta_{dry} = 0$ for bubbly, slug intermittent and annular flow regimes; $\theta_{dry} = \theta_{strat} (\frac{G_{wavy} - G}{G_{wavy} - G_{strat}})^{0.61}$ for stratified-wavy flow; $\theta_{dry} = \theta_{strat} \frac{x}{x_{IA}} (\frac{G_{wavy} - G}{G_{wavy} - G_{strat}})^{0.61}$ for slug/stratified-wavy flow, in case $x < x_{IA}$ Flow patterns, stratified angle θ_{strat}, intermittent to annular quality transition x_{IA}, stratified to stratified-wavy flow transition G_{strat} and the stratified-wavy to intermittent and annular flow transition G_{wavy} are obtainable in the original reference. $h_{wet} = [(Sh_{nb})^3 + h_{cb}^3]^{1/3}$, with convective boiling heat transfer coefficient h_{cb} as in Thome and El Hajal (2004). $h_{nb} = 131 p_{red}^{-0.0063} (-\log_{10}(p_{red}))^{-0.55} M^{-0.5} q^{0.58}$ $S = 1$ for $x < x_{IA}$ $S = 1 - 1.14(\frac{d}{0.00753})^2 (1 - \frac{\delta}{\delta_{IA}})^{2.2}$ for $x \geq x_{IA}$, with δ_{IA} using the following δ expression at the intermittent to annular flow transition. $\delta = \frac{d}{2} - \sqrt{(\frac{d}{2})^2 - \frac{\pi d^2 (1-\alpha)}{2(2\pi - \theta_{dry})}}$. In case of mist flow regime: $h_{mist} = 2 \cdot 10^{-8} \mathrm{Re}_H^{1.97} \mathrm{Pr}_V^{1.06} Y^{-1.83} \frac{\lambda_V}{d}$ $\mathrm{Re}_H = \frac{Gd}{\mu_V} [x + \frac{\rho_V}{\rho_L}(1 - x)]$ $Y = 1 - 0.1[(\frac{\rho_V}{\rho_L} - 1)(1 - x)]^{0.4}$ In case of dryout flow regime: $h_{dryout} = h(x_{di}) - \frac{x - x_{di}}{x_{de} - x_{di}} [h(x_{di}) - h_{mist}(x_{de})]$ $x_{di} = 0.58 \exp[0.52 - 0.236(\frac{G^2 d}{\rho_V \sigma})^{0.17} (\frac{G^2}{g\rho_V(\rho_L - \rho_V)d})^{0.17} (\frac{\rho_V}{\rho_L})^{0.25} (\frac{q}{q_{cr}})^{0.27}]$ $x_{de} = 0.61 \exp[0.57 - 0.502(\frac{G^2 d}{\rho_V \sigma})^{0.16} (\frac{G^2}{g\rho_V(\rho_L - \rho_V)d})^{0.15} (\frac{\rho_V}{\rho_L})^{-0.09} (\frac{q}{q_{cr}})^{0.72}]$ $q_{cr} = 0.131 \rho_V^{0.5} i_{LV} [g\sigma(\rho_L - \rho_V)]^{0.25}$	$0.6 \leq d \leq 10.06\ mm$ $80 \leq G \leq 1500\ kg\ m^{-2}s^{-1}$ $4 \leq q \leq 46\ kW\ m^{-2}$ $-28 \leq T_{sat} \leq 25\ ^\circ C$
Yun and Kim (2009)	$h = 16.26 \cdot q^{0.72} \cdot p_{red}^{0.88}$, for $\delta \geq \delta_{cr}$ $h = 1.09 \cdot 10^{-3} \frac{\lambda_V}{d} [\mathrm{Re}_{VO}(x + \frac{\rho_V}{\rho_L}(1 - x))]^{0.989} \mathrm{Pr}_V^{1.41} Y^{-1.15}$, for $\delta < \delta_{cr}$ $Y = 1 - 0.1[(\frac{\rho_V}{\rho_L} - 1)(1 - x)]^{0.4}$ $\delta = \frac{d}{2}(1 - \alpha^{0.5})$ $\delta_{cr} = (\frac{3}{4}(\frac{\mu_L}{\rho_L})^2 \frac{1}{g} \mathrm{Re}_L)^{1/3}$	$0.98 \leq d \leq 2.0\ mm$ $360 \leq G \leq 1500\ kg\ m^{-2}s^{-1}$ $18 \leq q \leq 40\ kW\ m^{-2}$ $0 \leq T_{sat} \leq 15\ ^\circ C$
Oh et al. (2011)	$h = Sh_{nb} + Eh_L$, with nucleate boiling heat transfer coefficient h_{nb} evaluated with Cooper (Cooper, 1984) expression. $S = 0.279(\phi^2)^{-0.029} Bo^{-0.098}$ $E = \max[(0.023\phi^{2.2} + 0.76), 1]$ $\phi^2 = 1 + \frac{C}{X} + \frac{1}{X^2}$, with the Chisholm parameter C set to 20, 12, 10 and 5 in case of liquid-vapor flow condition of turbulent-turbulent, laminar-turbulent, turbulent-laminar and laminar-laminar, respectively. $X = (\frac{f_L}{f_V})^{0.5} (\frac{1-x}{x})(\frac{\rho_V}{\rho_L})^{0.5}$, with $f = 16/\mathrm{Re}$ for laminar flows and $f = 0.049\mathrm{Re}^{-0.25}$ for turbulent flows. $h_L = 4.36 \frac{\lambda_L}{d}$ for $\mathrm{Re}_L < 230$ $h_L = \frac{(\mathrm{Re}_L - 1000)\mathrm{Pr}_L (\frac{f_L}{2})(\frac{\lambda_L}{d})}{1 + 12.7(\mathrm{Pr}_L^{2/3} - 1)(\frac{f_L}{2})^{0.5}}$ for $3000 \leq \mathrm{Re}_L \leq 10^4$ $h_L = \frac{\mathrm{Re}_L \mathrm{Pr}_L (\frac{f_L}{2})(\frac{\lambda_L}{d})}{1 + 12.7(\mathrm{Pr}_L^{2/3} - 1)(\frac{f_L}{2})^{0.5}}$ for $10^4 \leq \mathrm{Re}_L \leq 5 \cdot 10^6$ $h_L = 0.023 \mathrm{Re}_L^{0.8} \mathrm{Pr}_L^{0.4} (\frac{\lambda_L}{d})$ for $\mathrm{Re}_L \geq 5 \cdot 10^6$	$0.5 \leq d \leq 3.0\ mm$ $200 \leq G \leq 600\ kg\ m^{-2}s^{-1}$ $5 \leq q \leq 40\ kW\ m^{-2}$ $0 \leq T_{sat} \leq 20\ ^\circ C$ $fluids: CO_2, R134a, R22, R410A, R290$
Pamitran et al. (2011)	Same model as Oh et al. (2011), with a different evaluation of the enhancement and suppression factors: $S = 0.25(\phi^2)^{-0.2093} Bo^{0.7402}$ $E = \max[(0.009\phi^{2.2} + 0.76), 1]$	$1.5 \leq d \leq 3.0\ mm$ $50 \leq G \leq 600\ kg\ m^{-2}s^{-1}$ $5 \leq q \leq 70\ kW\ m^{-2}$ $0 \leq T_{sat} \leq 10\ ^\circ C$
Ducoulombier et al. (2011)	$h = \max([h_{nb}, h_{cb}])$, with nucleate boiling heat transfer coefficient evaluated with the model of Cheng et al. (2008) and Kim et al. (2004): $h_{cb} = h_{LO}(1.47 \cdot 10^4 Bo + 0.93(1/X_{tt})^{2/3})$, for $Bo > 1.1 \cdot 10^{-4}$ $h_{cb} = h_L(1 + 1.80(1/X_{tt})^{0.986})$, for $Bo < 1.1 \cdot 10^{-4}$ The liquid h_L and liquid-only h_{LO} heat transfer coefficients evaluated with Dittus and Boelter (1930) equation.	$d = 0.529\ mm$ $200 \leq G \leq 1200\ kg\ m^{-2}s^{-1}$ $10 \leq q \leq 30\ kW\ m^{-2}$ $-10 \leq T_{sat} \leq 0\ ^\circ C$
Fang (2013)	$h = 0.00061(S + E)\mathrm{Re}_L Fa^{0.11} \mathrm{Pr}_L^{0.4} [\log(\frac{1.024\mu_L}{\mu_{L,wall}})]^{-1} (\frac{\lambda_L}{d})$ where $\mu_{L,wall}$ is the liquid viscosity at the inner wall temperature and Fa is the Fang number, defined in Nomenclature. $S = 41000 Bo^{1.13} - 0.275$ $E = (\frac{x}{1-x})^a (\frac{\rho_L}{\rho_V})^{0.4}$ $a = 0.48 + 0.00524(\mathrm{Re}_L Fa^{0.11})^{0.85} - 5.9 \cdot 10^{-6} (\mathrm{Re}_L Fa^{0.11})^{1.85}$, for $(\mathrm{Re}_L Fa^{0.11}) < 600$ $a = 0.87$, for $600 \leq (\mathrm{Re}_L Fa^{0.11}) \leq 6000$ $a = 160.8 \cdot (\mathrm{Re}_L Fa^{0.11})^{-0.6}$, for $(\mathrm{Re}_L Fa^{0.11}) > 6000$	$0.529 \leq d \leq 7.75\ mm$ $97.5 \leq G \leq 1400\ kg\ m^{-2}s^{-1}$ $3.93 \leq q \leq 40\ kW\ m^{-2}$ $-40 \leq T_{sat} \leq 26.8\ ^\circ C$
Fang et al. (2017)	$h = F_f M^{-0.18} Bo^{0.98} Fr_L^{0.48} Bd^{0.72} (\frac{\rho_L}{\rho_V})^{0.29} [\log(\frac{\mu_L}{\mu_{L,wall}})]^{-1} Y (\frac{\lambda_L}{d})$ $Y = 1$, for $p_{red} \leq 0.43$ $Y = 1.38 - p_{red}^{1.15}$, for $p_{red} > 0.43$ $Fr_L = \frac{G^2}{gd\rho_L^2}$ $F_f = 2260$ for CO_2	$0.207 \leq d \leq 32\ mm$ $20 \leq G \leq 1500\ kg\ m^{-2}s^{-1}$ $1.99 \leq q \leq 140\ kW\ m^{-2}$ $0.043 \leq p_{red} \leq 0.61\ ^\circ C$

2.4 Two Phase Flow Corrugated Pipe Heat Transfer Coefficient Research

Cho and Kim [8] investigated the heat transfer and pressure drop properties of R744 during

evaporation within straight and microfin pipes.The micro-finned tube heat transfer coefficient is determined by Yun et al. [9] found a mean deviation of 38.09%.

The test conditions and studies of Cho and Kim are listed below.

Table 2.2. Test Conditions of Cho and Kim Studies [8]

Test conditions

Parameter	Value
Mass flow rate (kg $m^{-2} s^{-1}$)	212, 318, 424, 530, 656
Heat flux (kW m^{-2})	6, 12, 16, 20
Evaporation temperature (°C)	0, 5, 10, 20

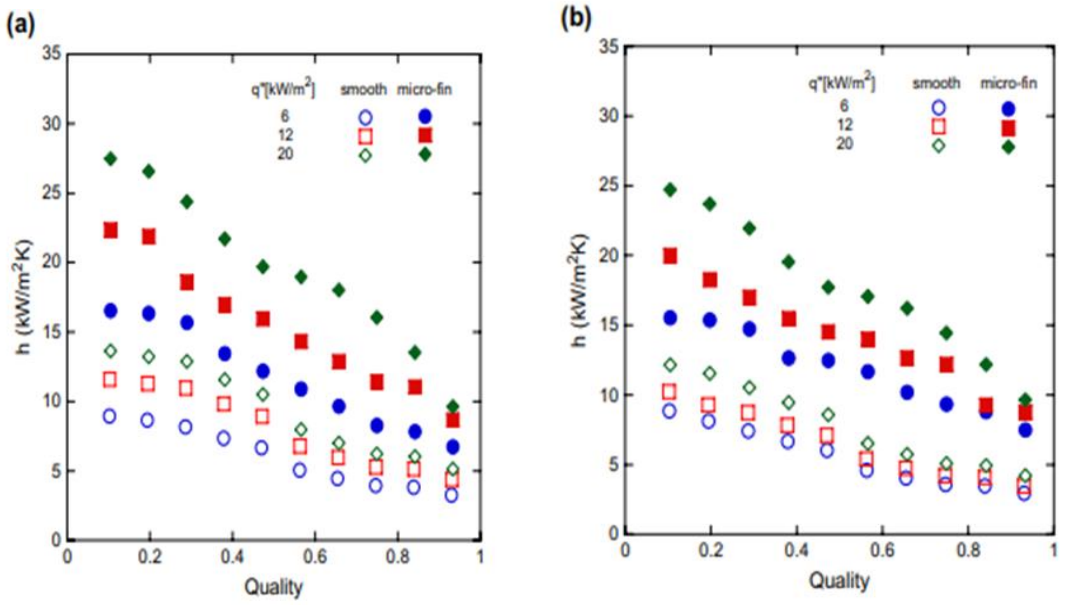

Figure 2.2, 2.3. Heat transfer coefficient vs quality scatter graph for different heat fluxes at the G=424 kg m^{-2} s^{-1} T_{sat}=0°C. a) D_{out}=5mm. b) D_{out} =9.52mm. [8]

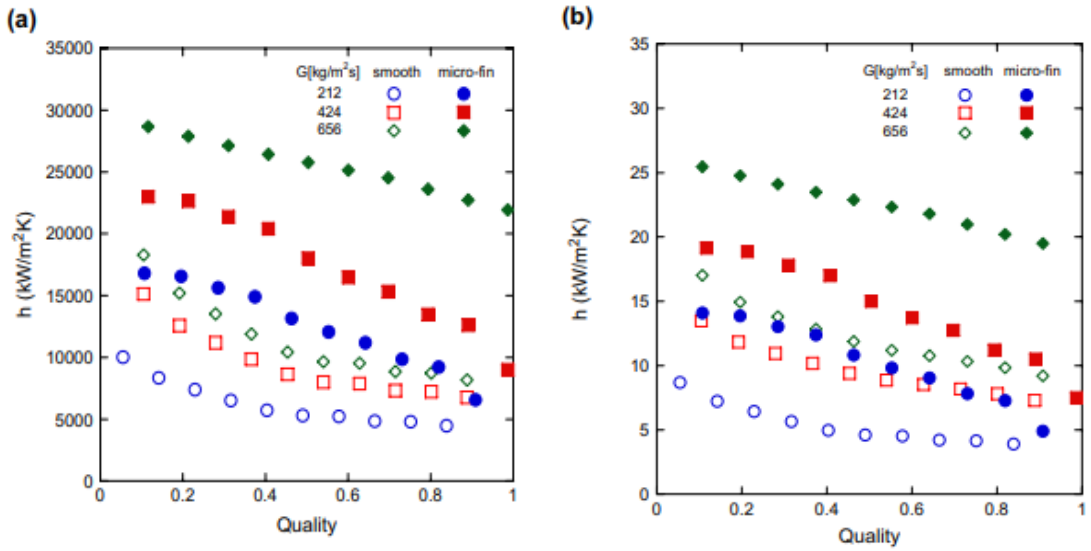

Figure 2.4., 2.5. Heat transfer coefficient vs quality scatter graph for different mass flux at the $\dot{Q}$=16 kW m^{-2} and T_{sat}=0°C. a) D_{out}=5mm. b) D_{out} =9.52mm. [8]

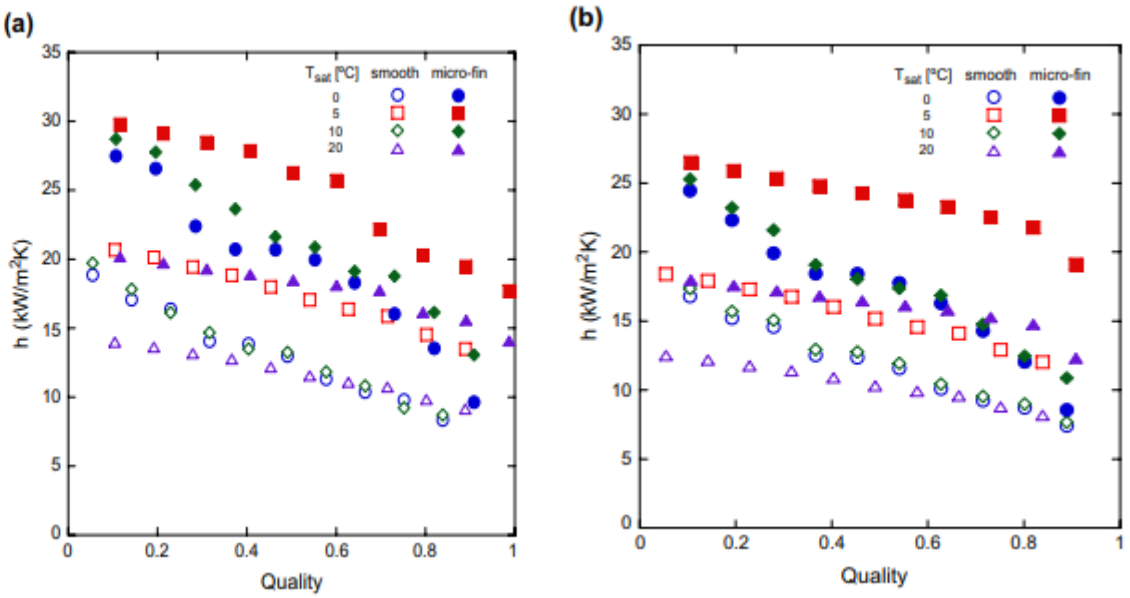

Figure 2.6., 2.7. Heat transfer coefficient vs quality scatter graph for different evaporating temperature at the $\dot{Q}$=20 kW m^{-2} and G=424 kg m^{-2} s^{-1}. a) D_{out}=5mm. b) D_{out} =9.52mm. [8]

The pressure drop of the micro-finned pipe was compared with the Chisholm parameter [10] and a deviation of 20%-70% was found.

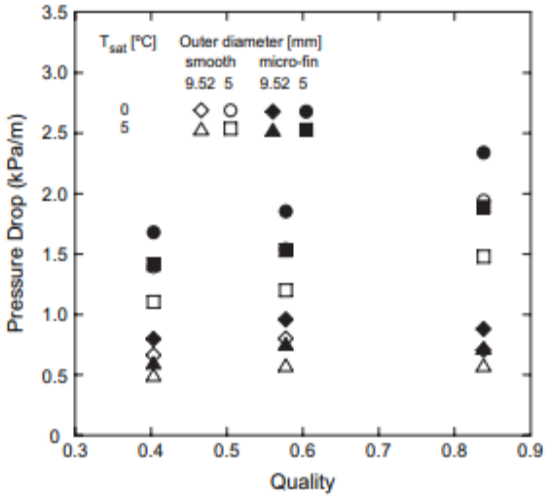

Figure 2.8. Pressure drop vs quality graph at the $\dot{Q}$ =12 kW m^{-2} and G=318 kg m^{-2} s^{-1}. [8]

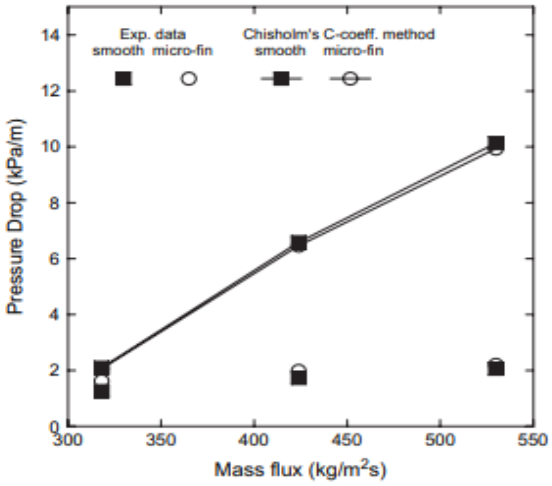

Figure 2.9. Pressure drop vs different mass flux graph (Comparison of exp. ΔP with Chisholm's C-coeff. method (1983) (D_{out}=5mm, q''=12 kW m^{-2}, T_{sat}=5°C). [8]

Mastrullo et al. [11] published a very comprehensive literature review in 2019. In this study, almost all studies that mention the evaporation of pure CO2 in horizontal and round pipes with surface treated (micro-finned and grooved) were scanned.

In these studies, different thread geometries, tube diameters, mass fluxes, heat fluxes and saturation temperatures were discussed. The authors provided the data for all these studies with Wu et al. With correlation by [12] estimating the heat transfer coefficient when CO2 evaporates purely in microfinned pipes (0ºC helix angle), Cheng et al. [13] with the improved correlation for grooved pipes by Rollman and Spindler [14] for R407C and R410A for straight pipes, and with the improved correlation by Mehendale [15] for microfin pipes with 2622 data points and 9 different fluids. . According to the results, Wu et al. Although [12] included the micro-fin effect in the correlation, the experimental data were not well predicted by this correlation (mean margin of error 163%). On the other hand, the Rollmann and Spindler [14] correlation averaged 58.9% margin of error, the Mehendale [15] correlation 30.5% mean margin of error, and Cheng et al. [13] correlation showed 41.4% margin of error.

Although there are two-phase studies, single-phase flow modeling has been done in this project, since it is a very complex flow for modeling. It is purposed to see the effect of finned surface on the heat transfer and pressure drop and one is selecting most optimum fin type.

3.MATERIAL AND METHOD

In this project, the fluid side of corrugated pipe geometry of a CO2 evaporator will be modeled using the CFD (Computational Fluid Dynamics) approach. Due to its high thermal conductivity and ease of processing, it was considered appropriate to choose the pipe material as copper. Since the diameter of the pipes is equivalent to the pipes in the industry, it is planned to have a 5/16" twisted and corrugated pipe structure.

Straight pipe and corrugated pipe will be compared according to heat transfer and pressure drop values. The modeled corrugated pipes will be modeled for three different parameters. Different apex and different helix are variable parameters.

Numerical models for various groove geometries will be created in the computer environment, mathematical equations and fluid side analyzes will be performed using ANSYS Fluent ® software licensed at Marmara University, and the model results will be

verified with theorical results.

As a CFD analysis program, ANSYS Fluent® solves conservation of mass and momentum using conservation of energy principles by discretizing it under boundary conditions for nonlinear quadratic equations. During the solution, a control volume-based technique is used. Turbulence models will be used in the flow solutions of the model.

Among them, standard k-$\boldsymbol{\varepsilon}$, k-ω, k-ω SST, realizable k-$\boldsymbol{\varepsilon}$ and RNG k-$\boldsymbol{\varepsilon}$ models are most preferred, but the method to be used is chosen depending on the heat exchanger being investigated. These turbulence models perform numerical analysis by solving the continuity, momentum and energy equations together [16].

The k-$\boldsymbol{\varepsilon}$ model is a model that allows solving the boundary layer with wall functions. Therefore, it provides a quick solution in flow types where the boundary layer does not need to be dissolved directly. Another computational model, k-omega, is a computational model mostly used in flows where boundary layer separations occur or in flows with sudden changes [17].

The computational model to be used in the project is the SST k-ω model. The SST k-ω model is a model designed to predict the location and amount of flow separation with high accuracy. It has been proven by numerous suitability studies that it performs successfully both in and out of the boundary layer in boundary layer simulations that require high accuracy. For turbulence modeling, suitable ones will be selected from the mentioned methods.

Continuity equation, momentum equation and energy equations will be solved together, and the result will be reached [18].

Conservation of mass and continuity equation:

$$\frac{\partial}{\partial t}(\alpha\rho_q) + \nabla.(\alpha_q\rho_q\vec{V}_q) = \sum_{p=1}^{n}\dot{m}_{pq} \tag{5}$$

Here, $\vec{V}_q$ is the velocity of phase q $\dot{m}_{pq}$ is the unit mass flow from phase p to phase q.

$$\begin{aligned}\frac{\partial}{\partial t}(\alpha_q\rho_q\vec{v}_q) + \nabla.(\alpha_q\rho_q\vec{v}_q\vec{v}_q) \\ = -\alpha_q\nabla\mathrm{p} + \nabla.\tau_q \\ + \sum_{p=1}^{n}(\vec{R}_{pq} + \dot{m}_{pq}\vec{v}_{pq}) + (\vec{F}_{lift,q} + \vec{F}_{vm,q} + \vec{F}_{vl,q} + \vec{F}_{td})\end{aligned} \tag{6}$$

Here, τq,q phase voltage-strain tensor is given in the formula below.

$$\tau_q = \alpha_q\mu_q[(\nabla\vec{v}_q - \nabla\vec{v}_q{}^T)] \tag{7}$$

Here, μ_q is the shear viscosity of phase q. $\vec{R}_{pq}$is the interaction force between phases.

p is the pressure shared between all phases. $\vec{v}_{pq}$ is the interface speed. $\vec{F}_{lift,q}$is the lift force. $\vec{F}_{vm,q}$ is the true mass force and $\vec{F}_{td}$ is the turbulent distribution force.

To define the energy conservation in the Eulerian multiphase model, the separated enthalpy equation could be written for each phase.

$$\frac{\partial}{\partial t}(\alpha_q\rho_q h_q) + \nabla.(\varphi_q\rho_q\vec{v}_q h_q) = -\tau_q{:}\nabla\vec{v}_q - \nabla\vec{q}_q + \sum_{p=1}^{n}(Q_{pq} + \dot{m}_{pq}h_{pq}) + S_q \tag{8}$$

The refrigerant side heat transfer coefficients and pressure losses of the corrugated tube heat exchangers will be calculated by MATLAB using the correlation equations that emerged as a result of the literature research.

After creating an module that can make parametric calculations on the MATLAB platform, the straight pipe will be modeled with the CFD method and the model will be tried to be verified with parametric calculation results. The heat transfer coefficient and pressure drop results of model results will be compared with parametric calculation results. After, models with different groove geometries will be created. Numerical solutions of these models will be made and they will be compared with correlations and straight pipe results of ANSYS.

4. RESULTS AND DISCUSSION

4.1. Physical Approach to Analysis

The increase in the heat transfer coefficient described by two different reasons (Cavallini et al. 2000) which are increasing the heat transfer surface and turbulence effect on the film surface.

It is the reality that the grooved surface can pass the liquid from the laminar locale to the turbulent locale quicker. Heat exchange and pressure drop improvements are for the most part because of the fundamental rising within the effective exchange zone and moreover to the turbulence actuated within the fluid film by the small scale balances and to the surface pressure impact on the condensate waste. [30]

For heat transfer improvements, in micro-finned tube, there are for the most part three fundamental mechanisms which are bigger successful heating area, drainage impact by surface tension and turbulent impact by micro-fin. [8]

The pressure drop is expressed as the pressure summation difference between the two focuses of a fluid transport pipe network. Pressure drop occurs when a resistance to flow occurs, in other words, when friction forces exist. The most determinant friction against liquid flow is the velocity of the liquid passing through the pipe and the viscosity of the liquid. The pressure drop increases according to the friction shear forces within the piping which are high degree of relative roughness, pipe fittings, joints, turns, grooved surface etc. [32]

4.2. Cad Modeling and Boundary Conditions

In this study, to see the effect of increasing heat transfer surface, for 3 different apex and 3 different helix angles, corrugated pipe CAD models are created. To simulate more accurate the case, just the fluid domain of the pipes is created. For 3 different Reynolds number (9000,12000,15000) which are turbulent flows, simulation boundary conditions determined. Below table represents simulation constant boundary conditions for three different Reynolds numbers.

Table 4.1. Ansys Simulation Constant Design Conditions

D_inner[mm]	**8 mm**
L[mm]	1000 mm
$\dot{Q}$ [heat in Watt]	300 W
T_inlet[°C]	-10

After giving the constant heat flux and inlet temperature, for every Reynolds number, by using steady state heat transfer formula and Dittus-Boelter correlation, saturation temperature of CO_2 is iterated. This iteration is performed with using MATLAB program 100 times. Following calculations represents one of the iterations to reach exact saturation temperature and it is done for all three Re values.

T_sat =0; (first assumption for T_sat of CO_2 in Celsius)

T_i=-10; %inlet temperature of the fluid in Celsius

D = 0.008; %pipe diameter in meter

$\dot{Q}$ =300; %heat given on the tube in Watt

L=1; %length of the tube in meter

A_s=pi*D*L; %heat flux surface area

A_c=pi*D^2/4; %cross sectional area of the tube in m^2

$\dot{q}$ =$\dot{Q}$/ A_s; %heat flux in W/m^2

Re=9000; %Reynolds number

$\dot{m}$=Re*μ*A_c/D; %mass flow rate in kg/s

V=$\dot{m}$/(ρ *A_c); %average velocity of the fluid in m/s

T_e=T_i+$\dot{Q}$/($\dot{m}$*c_p); %exit temperature in Celsius on the centerline of the tube

Nu=0.023*Re^0.8*Pr^0.4; %Dittus-Boilter Nusselt number correlation

h=Nu*k/D; %heat transfer coefficient in W/m^2.K

T_s=T_e+$\dot{Q}$/(A_s*h); %max. surface temperature of the exit in Celsius

T_s=(T_i+T_e)/2;

For all Re MATLAB coding (apx [1]) is done and with respect to these saturation temperatures CO_2 fluid properties is taken from REPROF [27] and shown below table.

Table 4.2. Properties of CO_2 at Saturation Temperatures -4°, -2.5°, 0°

	CO2 Fluid Properties at Liquid Form				
	ρ[kg/m^3]	c_p[J/kg.K]	k[W/m.K]	Pr	μ[Pa.s]
T_sat=-4°	950.63	2432.20	0.1139	2.2960	0.0001075
T_sat=-2.5°	942.11	2470.40	0.1121	2.3096	0.0001048
T_sat=0°	927.43	2542.30	0.1092	2.3385	0.0001004

For Re=9000 ⟶ T_sat=0° ⟶ V_axial=0.1218 m/s

For Re=12000 ⟶ T_sat=-2.5° ⟶ V_axial=0.1669 m/s

For Re=15000 ⟶ T_sat=-4.5° ⟶ V_axial=0.2121 m/s

Then by using ANSYS Design Modeler Module, cad model of the corrugated pipe fluid domain for different apex and helix angles and cad model of straight pipe are created.

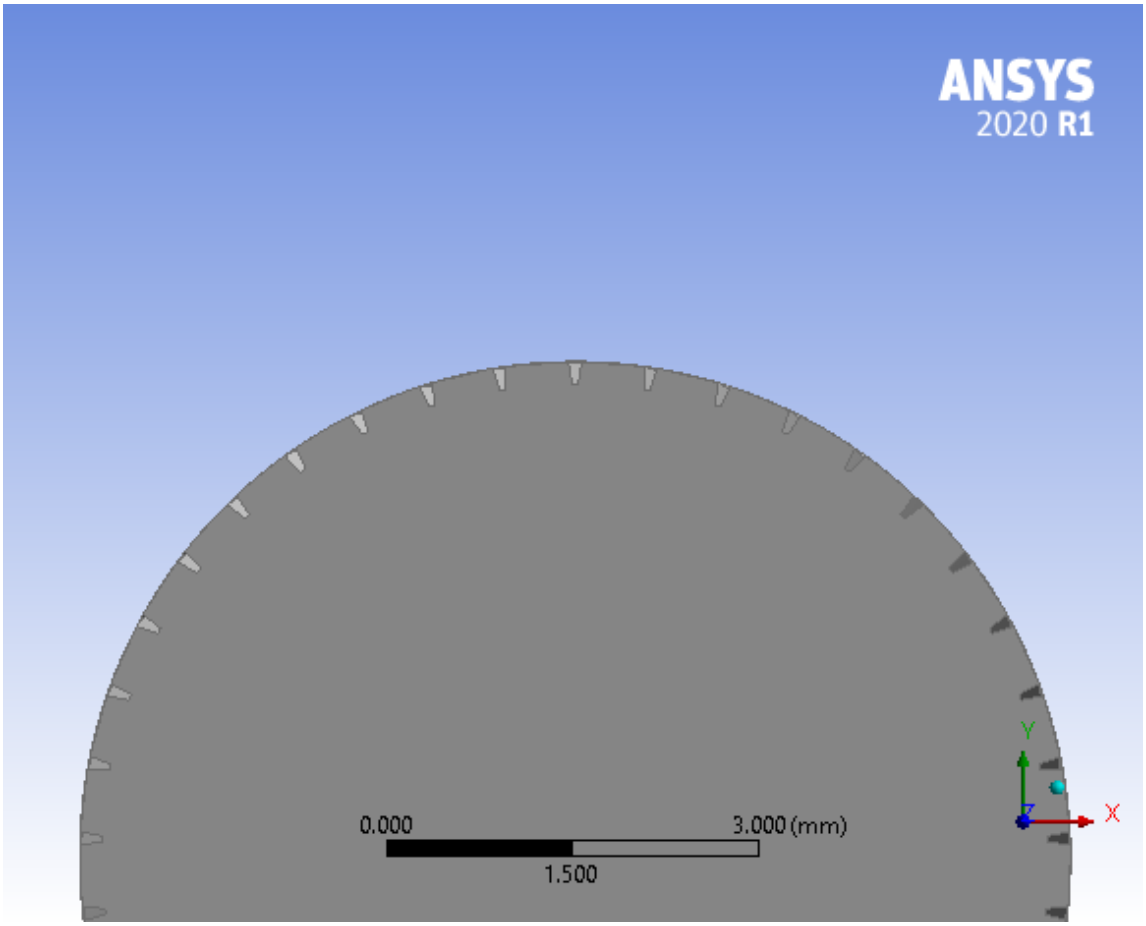

Figure 4.1. 18 apex 10 turns 40 fin Re 9000 Corrugated pipe fluid domain front view

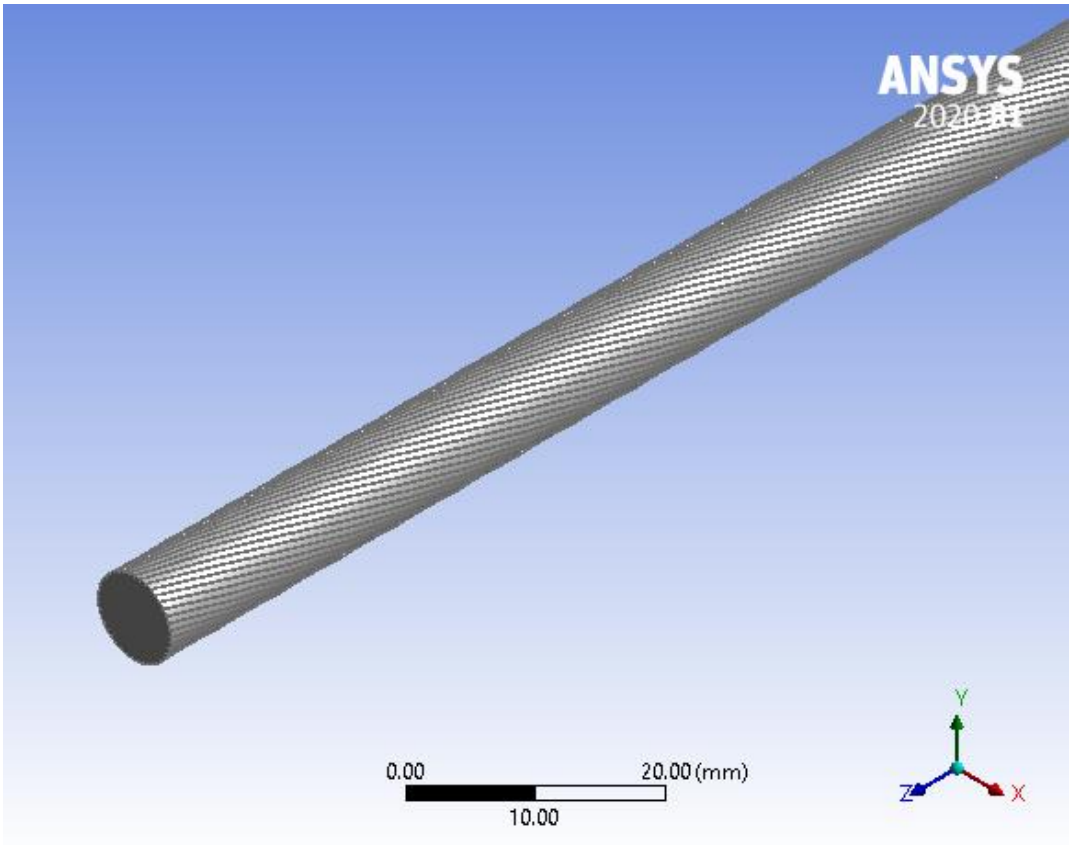

Figure 4.2. 18 apex 10 turns 40 fin Re 9000 Corrugated pipe fluid domain Isometric view

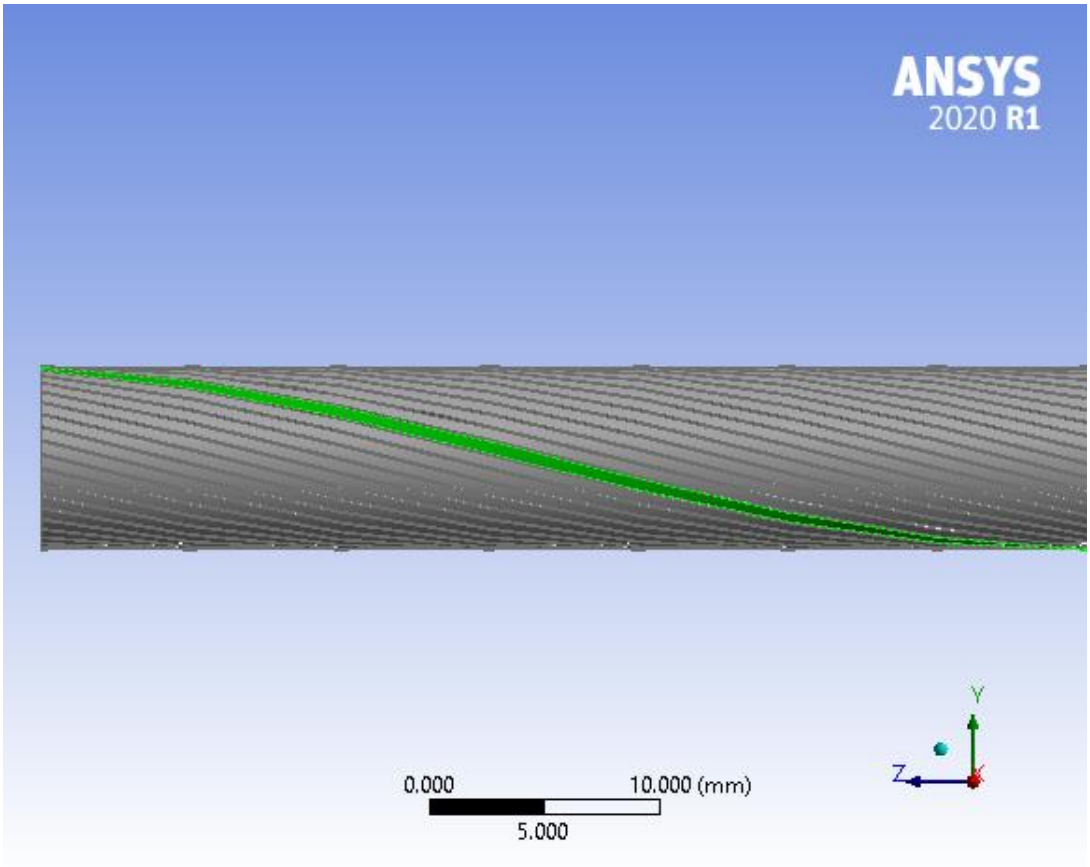

Figure 4.3. 18 apex 10 turns 40 fin Re 9000 Corrugated pipe fluid domain right view

To calculate the helix angle, trigonometric calculations is done. For 10 turns model, half of the one turn begins Z axis 0 mm and ends Z axis 10 mm. Also, it is also known Y axis which is length of the diameter. So, the helix angle is;

$$tan^{-1}(\frac{8}{50}) = 9°$$

Other helix angles are calculated at same method. Fin height is taken same for all models which is h=0.18mm. In addition, for each finned tube, 40 number of fins is created due to the restriction of computer capacities.

Note: Detailed drawings of corrugated pipes given in appendices number [2],[3],[4],[5],[6],[7]

4.3. Meshing Part

After the construction of the CAD models, meshing part is performed. Element size is given 0.00050003 m and number of nodes is 1196860, number of elements is 1033618. Then named selections is given as inlet surface of the pipe as Inlet, outlet surface of the pipe as Outlet, outer surface of the pipe as Heated-Wall and 3D volume of the pipe named as Fluid-Domain.

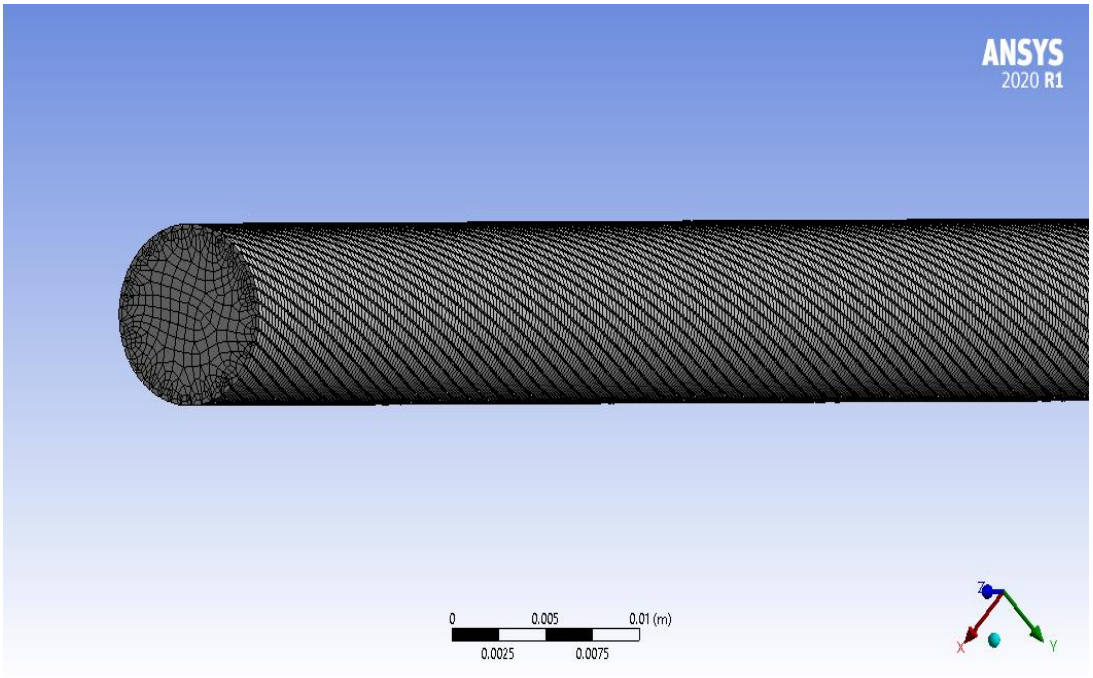

Figure 4.4. Meshing view of 18 apex 10 turns 40 fin Re 9000 Corrugated pipe

To see the mesh independence for 18 apex 10 turns 40 fin Re 9000 model, giving 3 different mesh element size, this model is dissolved and results are discussed.

4.4. Setup and Solution

At the setup part of the analysis, k-omega SST turbulence model is selected and energy equation is activated. At the general task page, time is assigned steady and gravity disabled. Because the model is horizontal and the pipe is fine, so it could be eliminated effect of the gravity.

Then from the Fluent Database, CO_2 properties is taken and changed with desired properties w.r.t. saturation temperatures that mentioned before.

Afterward, boundary conditions are given. Which are as follows:

Inlet ⟶ velocity inlet ⟶ axial velocity which is equal to for Re=9000⟶ 0.1218m/s

Outlet ⟶ pressure outlet ⟶ gauge pressure left by default which is 0 Pa

Heated-Wall⟶ wall ⟶ at he Thermal section heat flux is assigned which is equal to for Re=9000⟶ 11937W/m^2.K

Operating Conditions is taken as athmospheric pressure and gravity isn't activated.

Also reference values computed from inlet. At the residuals, absolute error rates determined for continuity, x-velocity, y-velocity, z-velocity, k, omega as 1e-04 and continuity absolute error is given as 1e-06.

Then hybrid initialization is done and at the calculation activities in the data file quantities, surface heat transfer coefficient and surface Nusselt number is added then for 1000 iterations solution is run.

Solution is done for all cases and the results are as follows:

4.5. Results (CFD Post Processing)

Results of the heat transfer coefficients and pressure drops is taken from CFD Post Processor by using function calculator. Heat transfer coefficient values are taken by using area average method on location heated wall and selecting variable as surface heat transfer coefficient. Pressure drop values are taken same method as area average on location inlet and selecting variable as pressure.

Table 4.3. Simulation Results W.R.T. Different Apex Angles

	Apex(β)	Helix(α)	Apex-Helix Angle	Corrugated Pipe h [W/m^2.K]	Corrugated Pipe ΔP [Pa]
1(#of fins 40) Re=9000	18°	9°	(18 9)	463.431	28.8
1(#of fins 40) Re=12000	18°	9°	(18 9)	587.428	50.7849
1(#of fins 40) Re=15000	18°	9°	(18 9)	705.692	77.9461
1(#of fins 40) Re=9000	20°	9°	(20 9)	451.014	24.7533
1(#of fins 40) Re=12000	20°	9°	(20 9)	575.412	43.6733
1(#of fins 40) Re=15000	20°	9°	(20 9)	699.068	66.7107
1(#of fins 40) Re=9000	22°	9°	(22 9)	429.193	26.2626
1(#of fins 40) Re=12000	22°	9°	(22 9)	548.543	46.3235
1(#of fins 40) Re=15000	22°	9°	(22 9)	662.749	70.9689

Table 4.4. Simulation Results W.R.T. Different Helix Angles

	Apex(β)	Helix(α)	Apex-Helix Angle	Corrugated Pipe h [W/m^2.K]	Corrugated Pipe ΔP [Pa]
1(#of fins 40) Re=9000	20°	5°	(20 5)	467.187	26.6939
1(#of fins 40) Re=12000	20°	5°	(20 5)	580.071	46.9336
1(#of fins 40) Re=15000	20°	5°	(20 5)	719.566	70.813
1(#of fins 40) Re=9000	20°	9°	(20 9)	451.014	24.7533
1(#of fins 40) Re=12000	20°	9°	(20 9)	575.412	43.6733
1(#of fins 40) Re=15000	20°	9°	(20 9)	699.068	66.7107
1(#of fins 40) Re=9000	20°	13.5°	(20 13.5)	431.317	24.0258
1(#of fins 40) Re=12000	20°	13.5°	(20 13.5)	546.218	42.5959
1(#of fins 40) Re=15000	20°	13.5°	(20 13.5)	661.455	65.4511

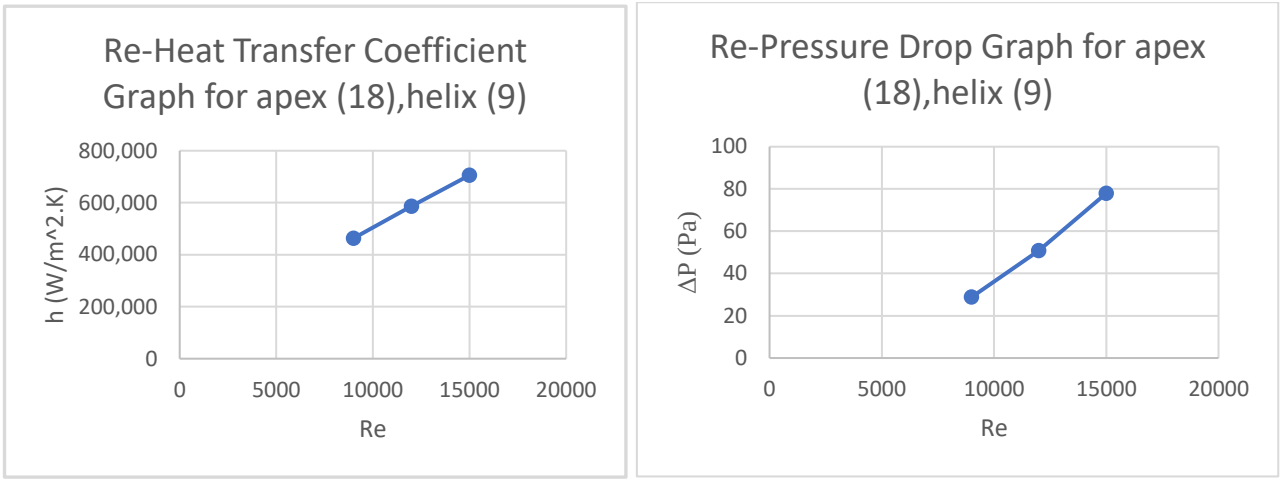

Figure 4.5., 4.6. Re-h and Re-ΔP Graph of Apex 18°-Helix 9°

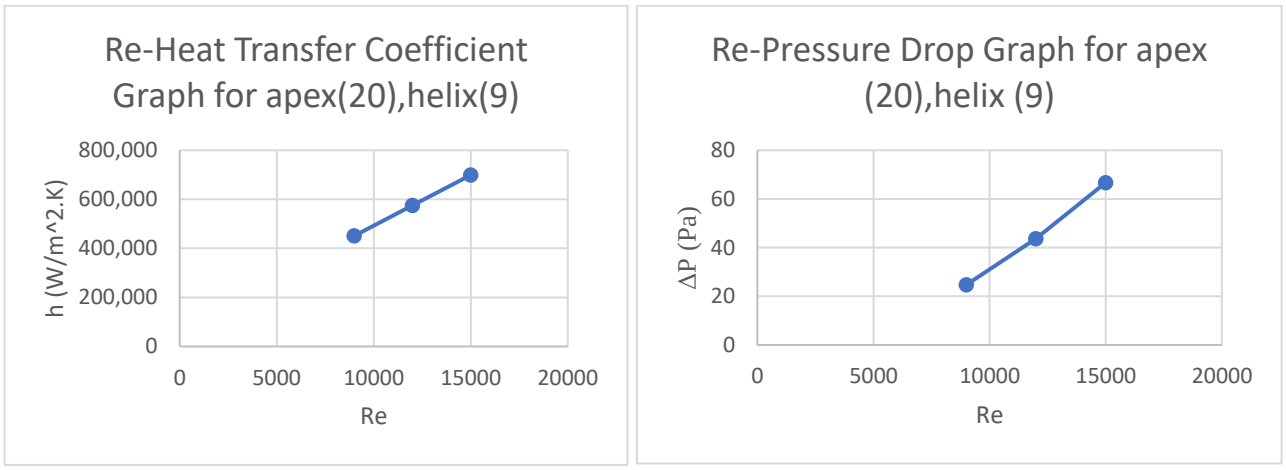

Figure 4.7., 4.8. Re-h and Re-ΔP Graph of Apex 20°-Helix 9°

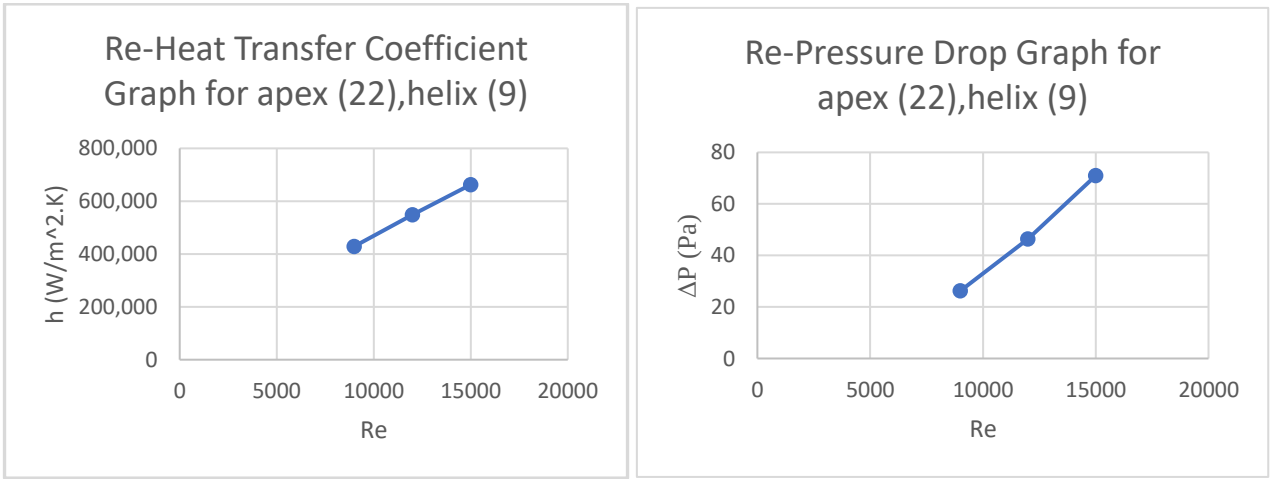

Figure 4.9., 4.10. Re-h and Re-ΔP Graph of Apex 22°-Helix 9°

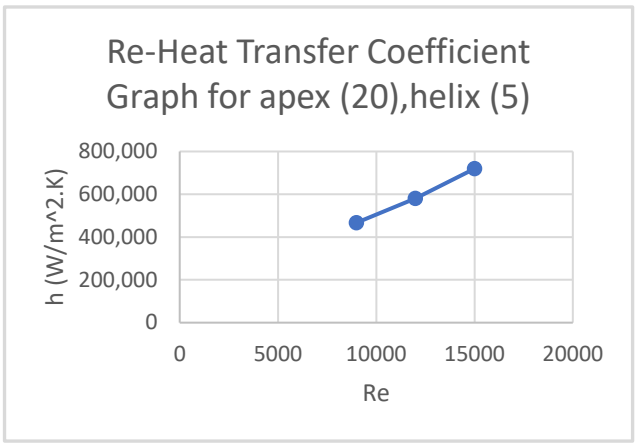

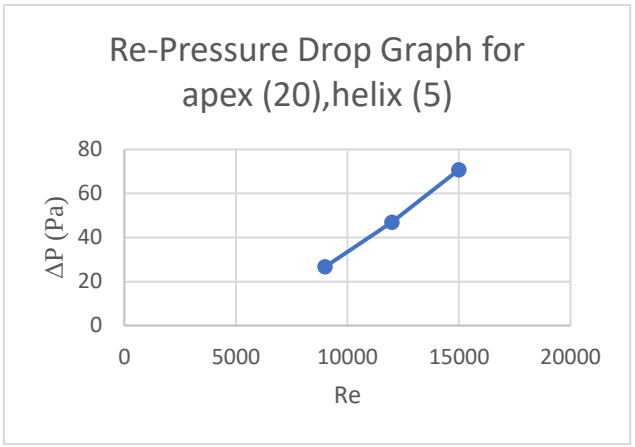

Figure 4.11., 4.12. Re-h and Re-ΔP Graph of Apex 20°-Helix 5°

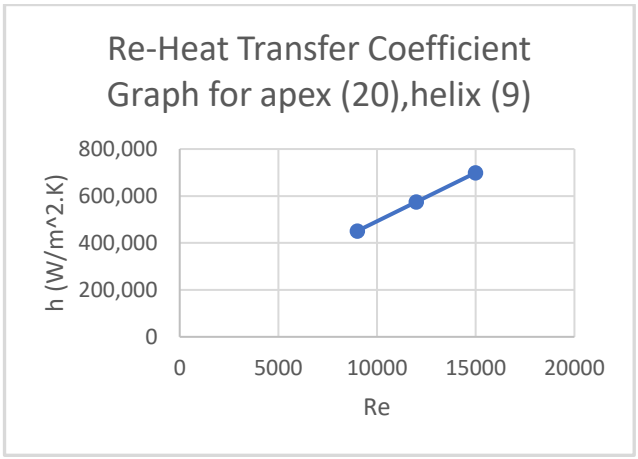

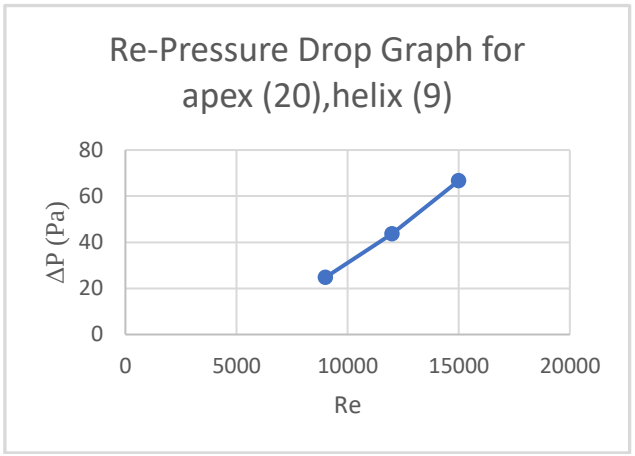

Figure 4.13., 4.14. Re-h and Re-ΔP Graph of Apex 20°-Helix 9°

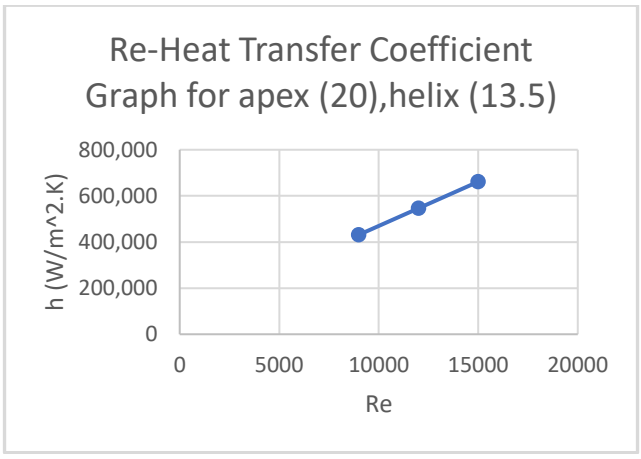

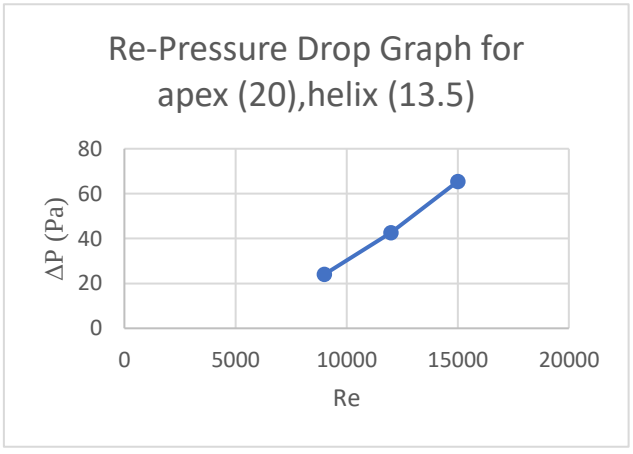

Figure 4.15., 4.16. Re-h and Re-ΔP Graph of Apex 20°-Helix 13.5°

Details of "Mesh"

Display	
Display Style	Use Geometry Setting
Defaults	
Physics Preference	CFD
Solver Preference	Fluent
Element Order	Linear
Element Size	5.0003e-004 m
Export Format	Standard
Export Preview Surface Mesh	No
Sizing	
Quality	
Inflation	
Assembly Meshing	
Advanced	
Statistics	
Nodes	1196860
Elements	1033618

h	463.43
ΔP	28.8

Details of "Mesh"

Display	
Display Style	Use Geometry Setting
Defaults	
Physics Preference	CFD
Solver Preference	Fluent
Element Order	Linear
Element Size	5.0003e-003 m
Export Format	Standard
Export Preview Surface Mesh	No
Sizing	
Quality	
Inflation	
Assembly Meshing	
Advanced	
Statistics	
Nodes	471885
Elements	421652

h	452.6
ΔP	26.1

Details of "Mesh"

Display	
Display Style	Use Geometry Setting
Defaults	
Physics Preference	CFD
Solver Preference	Fluent
Element Order	Linear
Element Size	5.0003e-002 m
Export Format	Standard
Export Preview Surface Mesh	No
Sizing	
Quality	
Inflation	
Assembly Meshing	
Advanced	
Statistics	
Nodes	471885
Elements	421652

h	449.56
ΔP	26.09

Figure 4.17. Mesh independence results (h in [W/m^2.K] ΔP in [Pa])

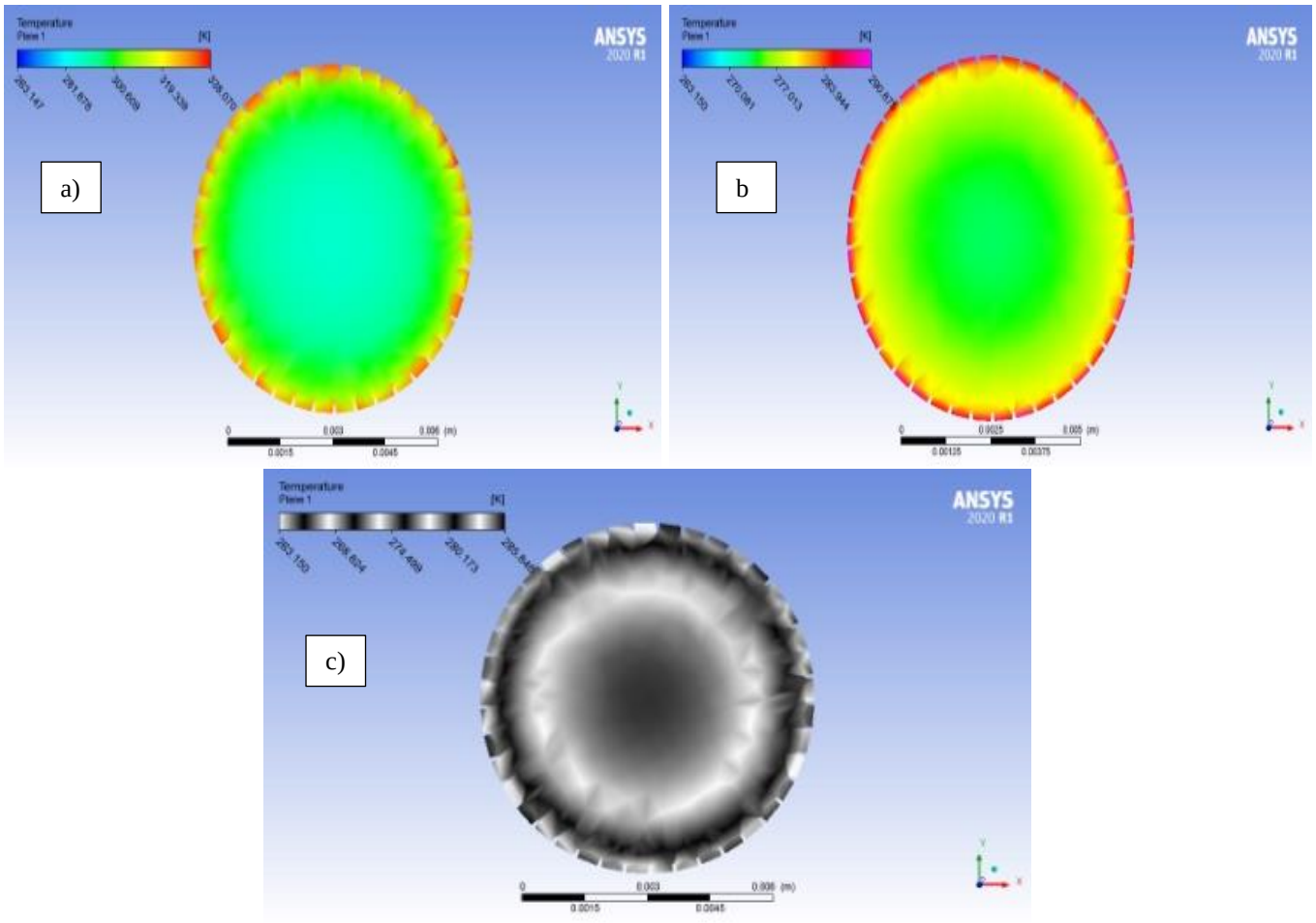

Figure 4.18. a) Temp. Distribution of apex 18° helix 9° Re 9000 **b)** Temp. Distribution of apex 18° helix 9° Re 12000 **c)** Temp. Distribution of apex 18° helix 9° Re 15000

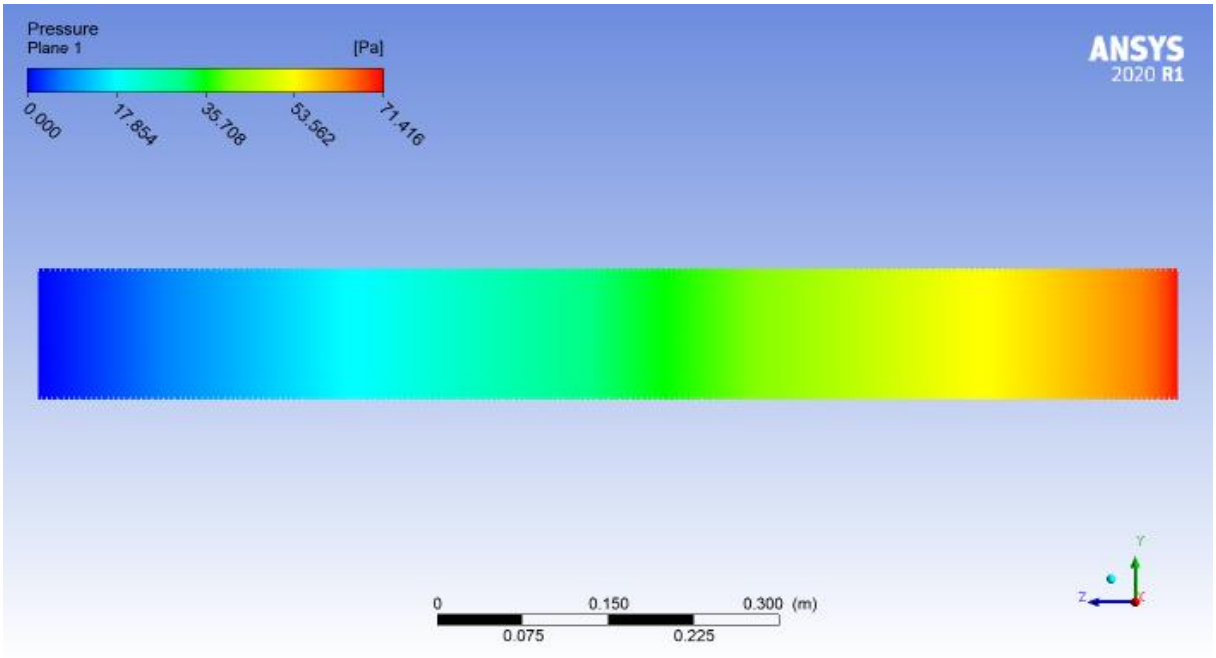

Figure 4.19. Pressure distribution plane for apex 20° helix 5° Re 15000

Table 4.5. Results of Straight Pipe Analysis, Correlations and Average Corrugated Pipe Analysis

Re	Straight Pipe h [W/m^2.K]	Straight Pipe ΔP [Pa]	Dittus–Boelter h [W/m^2.K]	Gnielinski h [W/m^2.K]	Blasius ΔP [Pa]	Avg. Corr. h [W/m^2.K] at Re=9000	Avg. Corr. ΔP [Pa] at Re=9000
9000	419.36	21.75	665.13	626.47	29.07	450.27	26.58
12000	532.17	41.68	826.19	801.61	49.52	568.67	45.66
15000	647.25	62.95	966.29	954.03	74.46	691.33	69.77

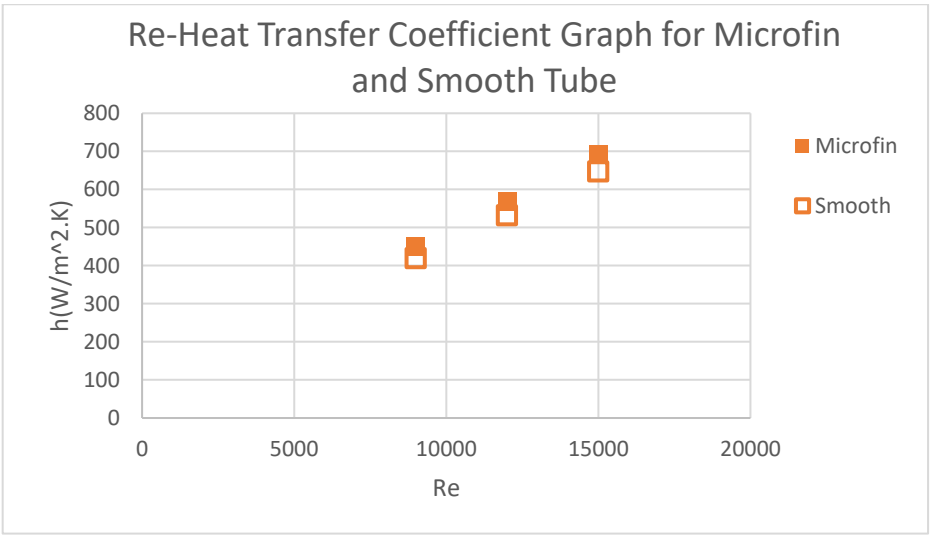

Figure 4.20. Re-h Graph of Micro-finned and Smooth Tube

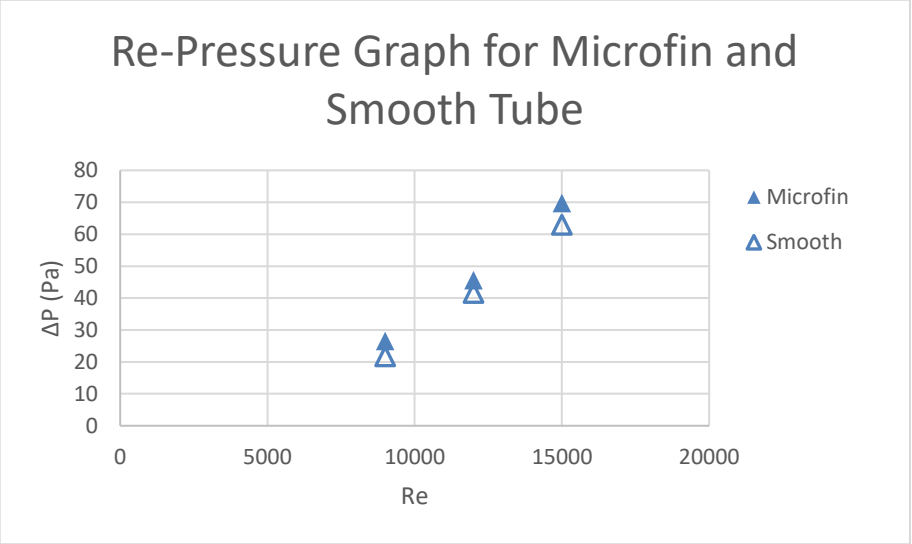

Figure 4.21. Re-ΔP Graph of Micro-finned and Smooth Tube

4.6. Discussion of the Results

When discussing the results in terms of mesh independence, it is seen that, results of heat transfer coefficients and results of pressure drop values same with very small difference. In other words, after a point, no matter how much improved the mesh, the result will not change. The aim is sort of, it actually gives the same result in bad mesh as in good mesh up to a point. It gives the same in different mesh quality, it could be said that mesh independent.

Another purpose of this analysis is to understand impact of finned surface on heat transfer coefficient and pressure drop. It is obvious that, corrugated pipe has higher heat transfer coefficient than straight pipe however vice versa for pressure drop.

In the Cho and Kim's test results, micro-finned tube has significantly higher heat transfer coefficients value from smooth tube. When comparing this study, it can be said that micro-finned tube has higher efficiency from the smooth tube however due to the computer restriction, at the geometry section, it could be just created 40 number of fins. In general, number of fins could be between 50 and 60. So, simulation results in terms of heat transfer coefficients are not effective comparing with the Cho and Kim's test results. On the other hand, analysis is successful regarding to see the difference more wetted portion promotes and surface area increases heat transfer coefficient. Comparing the pressure drop results with the Chisholm parameter, it is onto the same trend with the simulation results. Difference caused by different design conditions like pipe diameter, heat flux, mass flux, saturation temperature

etc.

When examine the results according to average values between corrugated and straight pipe results, it is seen that heat transfer coefficient value increases 7% and pressure drop increases 18.17% at Re equal to 9000. At the Reynolds 12000 and 15000, heat transfer increase slightly same with 9000. However, with the increase of Re, absolute error between corrugated and smooth pipe pressure drop decrease which are 15.84% at Re 12000 and 15.46% at Re 15000.

To examine the effect of Re on the temperature of the flowing fluid, it is added to Post processor part plane views of 18 apex 9 helix angle for 3 Re values. With increasing mass flow, exit temperature of the fluid decreases so, saturation of the fluid is decreasing. To see the pressure drop phenomena also, at the Post processor part pressure plane for 20 apex 5 helix Re 15000 model shared.

When comparing the theoretical results, there are difference more than 20 percent. It is due to fully developed phenomena. The analyzed flow is not fully developed but the correlations equations calculate the heat transfer and pressure drop assuming the flow is fully developed. For this reason, there are big difference. To minimize this situation, it is selected turbulence flow. Also, it is known that Dittus-Boelter correlation gives nearly 20% errors.

When looking up the results with respect to apex angle, the optimum degree is detected as 20°. At this apex angle, heat transfer coefficient and pressure drop values are optimum level. So, after the selection of apex angle which is 20°, changing the helix angle for that fin type, it is reached most optimum fin type. Consequently, the most optimal fin type is 20° apex angle and 5° helix angle.

In addition, we it could be easily seen the effect of Re on H.T.C. and pressure drop. As Re increases, H.T.C. and pressure drop increases as shown as with all Re-h and Re-ΔP charts.

5. CONCLUSION

Correctly verified corrugated pipe geometry will form the basis for efficiency studies in CO2 transcritical circulation cooling systems. If the study achieves its purpose, the currently used HFC gases will be replaced by more economical, environmentally, friendly and competitive CO2 gas in terms of performance. CO2 is economically the most suitable compared to other gases. Thanks to the system control elements, the current machine and heat exchanger

technology has reached competitive levels, especially in northern countries with R744 (CO2) efficiency in terms of transcritical cycle and in southern countries with subcritical cascade cycle.

Recently, the use of CO2 as a refrigerant in cold drink vending machines, supermarkets, cold rooms, food production and processing plants, industrial ice cream production machines, heat pumps and vehicle air conditioners has become increasingly common. Our country is one of the countries that will be most affected by a possible climate change, especially due to global warming. It brings many negative effects such as forest fires due to high temperatures, the decrease in the occupancy rate of the dams to critical levels, sudden weather changes and natural disasters, damage to agricultural products due to drought, and narrowing of the habitats of animals. In this sense, environmentally friendly industrial studies are very important. This prudent approach will expand our country's market share in other environmentalist countries and will leave a clean and livable world to future generations.

In this thesis study, all the theoretical information and correlations related to straight and corrugated pipes were reached and heat transfer coefficient and pressure drop calculations were calculated with the current and the most efficient correlations. Dittus-Boelter correlation and Gnielinski correlation were chosen as the most appropriate correlations in our study, and the theoretical heat transfer coefficient results were compared with the results of simulation. Straight pipes and corrugated pipes were modeled, and the heat transfer coefficient and pressure drop values were reached by help of the ANSYS Fluent.

The only negative factor for corrugated pipe is pressure drop. By changing the geometry properties of corrugated pipes, an optimum corrugated geometry with low pressure drop and high heat transfer coefficient is achieved. When looking at the results of the corrugated pipe model according to different apex (β) and helix (α) angles, it is understood that this optimum geometry can be obtained with an apex angle of 20 degrees and a helix angle of 5 degrees. This geometry has the highest heat transfer coefficient and the lowest pressure drop compared to other models.

According to the results obtained, it is understood that the use of corrugated pipes has a significant effect on the heat transfer coefficient despite the pressure drop. Maximum efficiency can be obtained from the corrugated pipes by choosing the combination of geometry with the highest heat transfer coefficient and the lowest pressure drop. As an advice, to reach the optimum selection, optimization tool could be used.

Finally, it is intended to effect of finned surface on the H.T.C. and pressure drop and investigated numerically. In the light of these findings, it is recommended to carry out an optimization study to optimize the relevant geometry, the effects of these geometric parameters on heat transfer.

6. REFERENCES

[1] Bellstedt, M., Elefsen, F., & Jensen, S. S. (2002). Application of CO2 (R744) refrigerant in industrial cold storage plant. EcoLibrium, 1(5), 25-30.

[2] Kasap, F., Acül, H., Canbaz, H., & Erbil, S. (2011). R744 (CO2) soğutucu akışkanlı soğutma sistemleri, kanatlı borulu R744 (CO2) evaporatör ve gaz soğutucu tasarım esasları. X. Ulusal Tesisat Mühendisliği Kongresi, 13-16 Nisan, İzmir, Türkiye.

[3] Kim, M. H., Pettersen, J., & Bullard, C. W. (2004). Fundamental process and system design issues in CO2 vapor compression systems. Progress in energy and combustion science, 30(2), 119-174.

[4] Refrigeration, D. Air Conditioning Division, Food Retail CO2 Refrigeration Systems, Danfoss A/S (RA Marketing/MWA). DKRCE. PA, 1.

[5] Lemmon, E. W., Huber, M. L., & McLinden, M. O. (2010). NIST standard reference database 23. Reference fluid thermodynamic and transport properties (REFPROP), version, 9.

[6] Fartaj, A., Ting, D. S. K., & Yang, W. W. (2004). Second law analysis of the transcritical CO2 refrigeration cycle. Energy conversion and Management, 45(13-14), 2269-2281.

[7] Ceran, L. (2010). Evaporatör ve kondenserlerde içten yivli boru kullanılmasının avantajları ve dezavantajlarının incelenmesi.

[8] Cho, J. M., & Kim, M. S. (2007). Experimental studies on the evaporative heat transfer and pressure drop of CO2 in smooth and micro-fin tubes of the diameters of 5 and 9.52 mm. International Journal of Refrigeration, 30(6), 986-994.

[9] Yun, R., Kim, Y., Seo, K., & Kim, H. Y. (2002). A generalized correlation for evaporation heat transfer of refrigerants in micro-fin tubes. International journal of heat and mass transfer, 45(10), 2003-2010.

[10] Chisholm, D. (2006). Two-phase flow in pipelines and heat exchangers, 1983. KIM, D.; GHAJAR, A. A General Heat Transfer Correlation for Non-Boiling Gas–Liquid Flow

with Different Flow Patterns in Horizontal Pipes. International Journal of Multiphase Flow, 32(4), 447-465.

[11] Mastrullo, R., Mauro, A. W., & Viscito, L. (2019). Flow boiling of carbon dioxide: Heat transfer for smooth and enhanced geometries and effect of oil. state of the art review. International Journal of Refrigeration, 108, 311-335.

[12] Wu, X., Zhu, Y., & Tang, Y. (2015). New experimental data of CO2 flow boiling in mini tube with micro fins of zero helix angle. international journal of refrigeration, 59, 281-294.

[13] Cheng, L., Ribatski, G., Quibén, J. M., & Thome, J. R. (2008). New prediction methods for CO2 evaporation inside tubes: Part I–A two-phase flow pattern map and a flow pattern based phenomenological model for two-phase flow frictional pressure drops. International Journal of Heat and Mass Transfer, 51(1-2), 111-124.

[14] Rollmann, P., & Spindler, K. (2016). New models for heat transfer and pressure drop during flow boiling of R407C and R410A in a horizontal microfin tube. International Journal of Thermal Sciences, 103, 57-66.

[15] Mehendale, S. (2018). A new heat transfer coefficient correlation for pure refrigerants and near-azeotropic refrigerant mixtures flow boiling within horizontal microfin tubes. International Journal of Refrigeration, 86, 292-311.

[16] Hellsten, A., Laine, S., Hellsten, A., & Laine, S. (1997). Extension of the k-omega-SST turbulence model for flows over rough surfaces. In 22nd Atmospheric Flight Mechanics Conference (p. 3577).

[17] Kalkan, O. O. (2014). Implementation of k-epsilon turbulence models in a two-dimensional parallel navier-stokes solver on hybrid grids. Middle East Technical University, Ankara, Turkey.

[18] Sadaghiani, A. K., & Koşar, A. (2016). Numerical and experimental investigation on the effects of diameter and length on high mass flux subcooled flow boiling in horizontal microtubes. International Journal of Heat and Mass Transfer, 92, 824-837.

[19] Çengel,Y.A.,Cimbala,J.M.,(2017).Fluid Mechanics: Fundamental and Applications ,4th Edition, McGraw-Hill Higher Education.

[20] Gnielinski V., (2013), “On heat transfer in tubes,” International Journal of

Heat and Mass Transfer", 63 (3) 134-140.

[21] Azeri,B.(2019) CO_2 Akışkanlı Soğutma Sistemlerinde Kullanılan Kanatlı Borulu Isı Değiştiricilerinin Termal Analizi.Yüksek Lisans Tezi,Gebze Teknik Üniversitesi,Fen Bilimleri Enstitüsü,Gebze,Türkiye

[22] Shah R. K., Sekulic D. P., (2004), "Fundamentals of heat technology", 3.

Baskı, John Wiley & Sons Inc. , 132-133.

[23] Dang C., Hihara E., (2004), "In-tube cooling heat transfer of supercritical carbon dioxide. Part 2. Comparison of numerical calculation with different turbulence models", International Journal of Refrigeration, 27 [3] 748-760.

[24] Ma Y., Liu Z., Tian H., (2013), "A review of transcritical carbon dioxide heat

pump and refrigeration cycles", Energy, 55 (3) 156-172.

[25] Santosa I. M. C., Gowreesunker B. L., Tassou S. A., Tsamos K. M., Ge Y., (2017), "Investigations into air and refrigerant side heat transfer coefficients of finned-tube CO2 gas coolers," International Journey of Heat and Mass Transfer, 107 (5) 168-180.

[26] https://trc.nist.gov/refprop/MINIREF/MINIREF.HTM

[27] Fang,X.,2013.A new correlation of flow boiling heat transfer coefficients for carbon dioxide.Int.J.Heat Mass Transf.64,802-807.

[28] Fang,X.,Wu,Q.,Yuan,Y.,2017.A general correlation for saturated flow boiling heat transfer in channels of various sizes and flow directions.Int J.Heat Mass Transf.107,972-981.

[29] Pettersen J.,2004.Flow vaporization of CO2 in microchannel tubes.Exp.Therm.Fluid Sci.28,111-121.

[30] CAVALLİNİ 2000, Heat transfer and pressure drop during condensation of refrigerants inside horizontal enhanced tubes A. Cavallini a, D. Del Col a , L. Doretti a , G.A. Longo b, L. Rosset

[32] https://en.wikipedia.org/wiki/Pressure_drop

APPENDICES

[1]

```
clear;
clc;
T_sat=0; %first assumption for T_sat of CO2
for i=1:100
    properties=xlsread('RefprofCoiki');
    xx=find(T_sat==properties(:,2));
    rho=properties(xx,4);
    c_p=properties(xx,6)*10^3;
    k=properties(xx,8);
    mu=properties(xx,10);
    Pr=properties(xx,12);
T_i=-10; %inlet temperature of the fluid in Celsius
D=0.008; %diameter in meter
Q_dat=300; %heat given on the tube
L=1; %length of the tube in meter
A_s=pi*D*L; %heat flux surface area
A_c=pi*D^2/4; %cross sectional area of the tube
q_dat=Q_dat/A_s; %heat flux in W/m^2
Re=9000; %Reynolds number
m_dat=Re*mu*A_c/D; %mass flow rate in kg/s
V=m_dat/(rho*A_c); %average velocity of the fluid in m/s
T_e=T_i+Q_dat/(m_dat*c_p); %exit temperature in Celsius on the centerline
of the tube
Nu=0.023*Re^0.8*Pr^0.4; %Dittus-Boilter Nusselt number correlation
h=Nu*k/D; %heat transfer coefficient in W/m^2.K
T_s=T_e+Q_dat/(A_s*h); %max. surface temperature of the exit in Celsius
T_sat=(T_i+T_e)/2-mod((T_i+T_e)/2,0.5);
i=i+1;
end
```

[2]

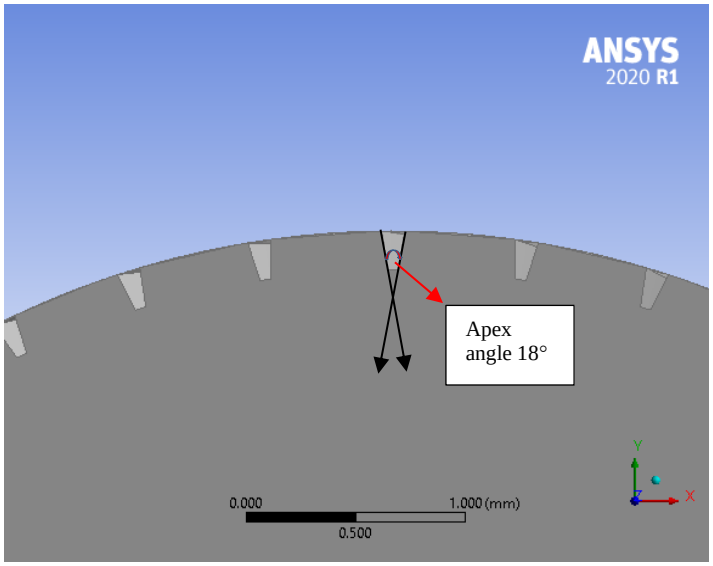
ANSYS
2020 R1
Apex
angle 18°
0.000
1.000 (mm)
0.500
Y
X

[3]

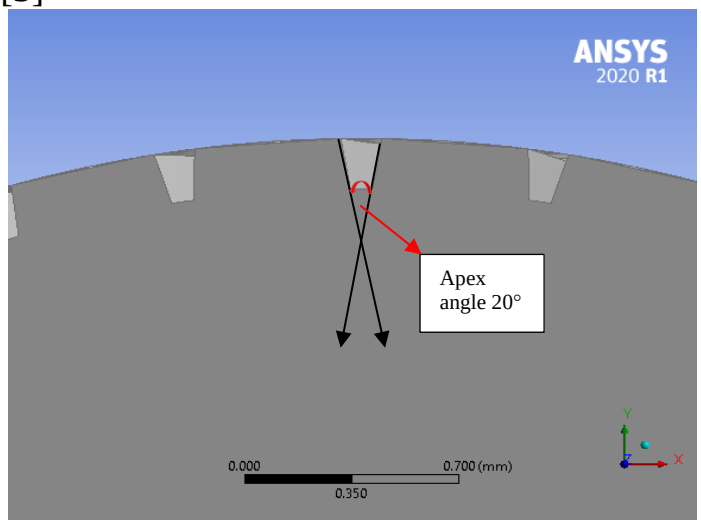
ANSYS
2020 R1
Apex
angle 20°
0.000
0.700 (mm)
0.350
Y
X

[4]

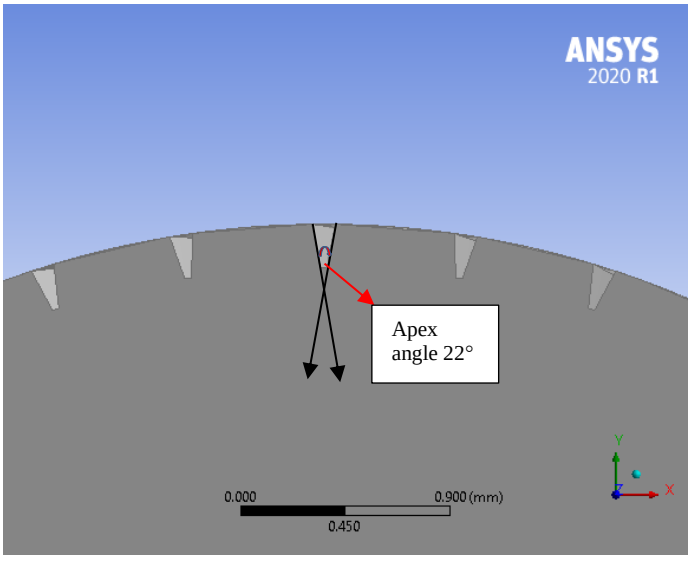
ANSYS
2020 R1
Apex
angle 22°
0.000
0.900 (mm)
0.450
Y
X

[5]

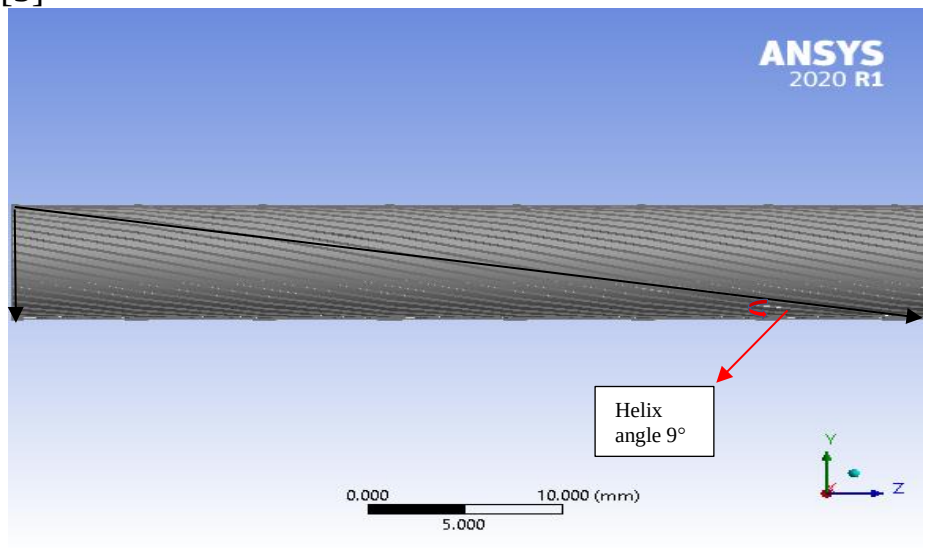
ANSYS
2020 R1
Helix
angle 9°
0.000
10.000 (mm)
5.000
Y
Z

[6]

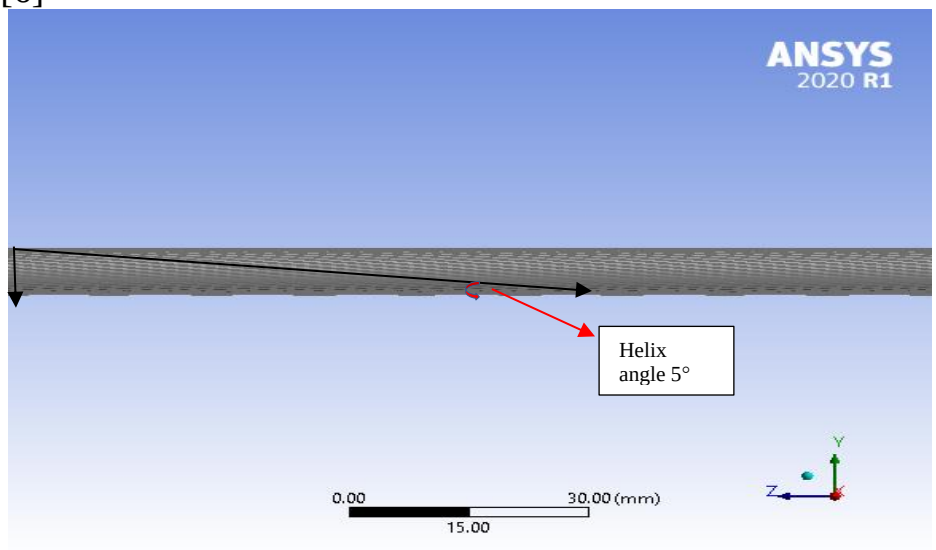
ANSYS
2020 R1
Helix
angle 5°
0.00
30.00 (mm)
15.00
Y
Z

[7]

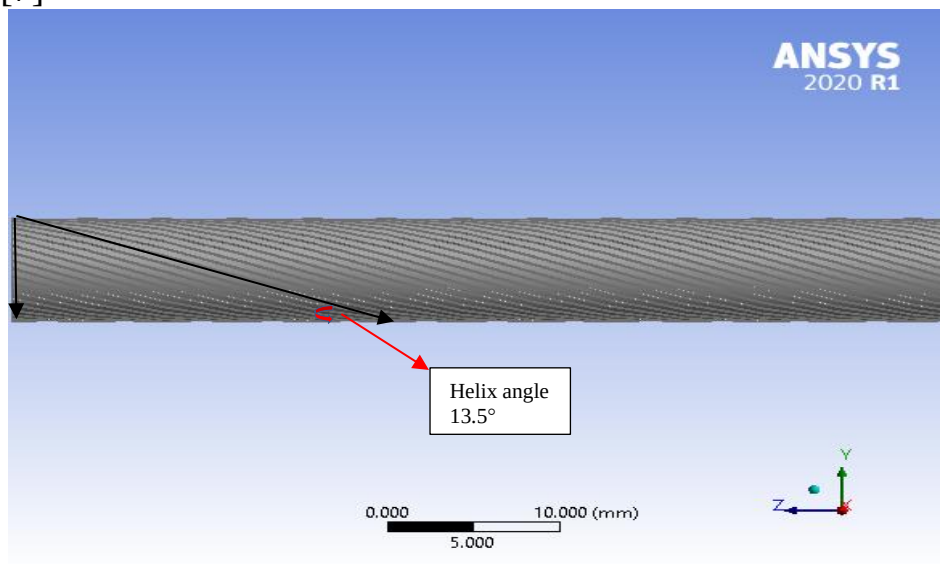
ANSYS
2020 R1
Helix angle
13.5°
0.000
10.000 (mm)
5.000
Y
Z